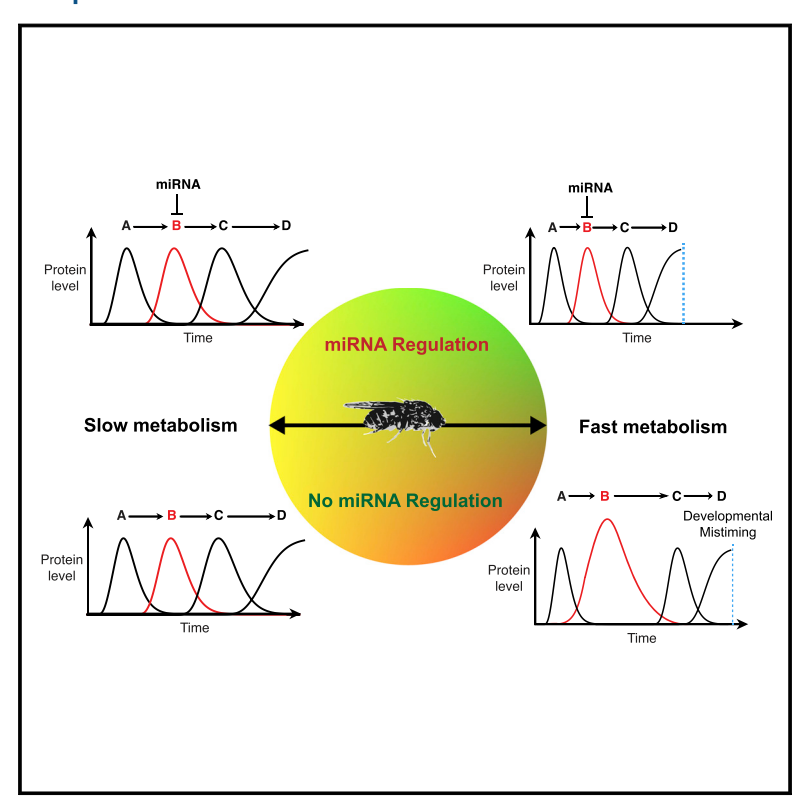


Repressive Gene Regulation Synchronizes Development with Cellular Metabolism

Graphical Abstract



Authors

Justin J. Cassidy, Sebastian M. Bernasek, Rachael Bakker, ..., Neda Bagheri, Luis A. Nunes Amaral, Richard W. Carthew

Correspondence

amaral@northwestern.edu (L.A.N.A.), r-carthew@northwestern.edu (R.W.C.)

In Brief

microRNAs become dispensable for development in the context of slower metabolism.

Highlights

- Cellular metabolic rate controls the tempo of development
- Multiple weak repressors allow GRN dynamics to adjust to a variable tempo
- Slow metabolism renders individual repressors redundant
- microRNAs become dispensable for development in the context of slower metabolism





Repressive Gene Regulation Synchronizes Development with Cellular Metabolism

Justin J. Cassidy,^{1,7,8} Sebastian M. Bernasek,^{2,3,7} Rachael Bakker,^{1,3} Ritika Giri,^{1,3} Nicolás Peláez,^{1,4} Bryan Eder,^{1,3} Anna Bobrowska,^{1,9} Neda Bagheri,^{2,3,5} Luis A. Nunes Amaral,^{2,3,5,6,*} and Richard W. Carthew^{1,3,10,*}

SUMMARY

Metabolic conditions affect the developmental tempo of animals. Developmental gene regulatory networks (GRNs) must therefore synchronize their dynamics with a variable timescale. We find that layered repression of genes couples GRN output with variable metabolism. When repressors of transcription or mRNA and protein stability are lost, fewer errors in Drosophila development occur when metabolism is lowered. We demonstrate the universality of this phenomenon by eliminating the entire micro-RNA family of repressors and find that development to maturity can be largely rescued when metabolism is reduced. Using a mathematical model that replicates GRN dynamics, we find that lowering metabolism suppresses the emergence of developmental errors by curtailing the influence of auxiliary repressors on GRN output. We experimentally show that gene expression dynamics are less affected by loss of repressors when metabolism is reduced. Thus, layered repression provides robustness through error suppression and may provide an evolutionary route to a shorter reproductive cycle.

INTRODUCTION

Animal development occurs over a defined timescale, which is an intrinsic feature of a species and not necessarily determined by external clocks (Ebisuya and Briscoe, 2018). Development occurs via a stereotypic sequence of events involving cell division, growth, movement, apoptosis, polarization, and differentiation. Correct assembly of functional structures depends on synchronization of cell division and differentiation events (Foe, 1989; Sulston et al., 1983). Small variation in timing produces variation in structure that is observed between individuals (Fran-

cesconi and Lehner, 2014; Poullet et al., 2016). Abnormal timing can result in structural defects that lead to compromised survival (Moss, 2007). Thus, the rates of various developmental processes must be controlled and coordinated.

Although developmental tempo is a fundamental property of a species, it can vary under different conditions. For example, temperature affects the pace of development in many ectotherms, such as arthropods, nematodes, fish, and reptiles (Atlas, 1935; Davidson, 1944; Kuntz and Eisen, 2014; Zuo et al., 2012). Diet and food intake also affect organismal growth rate and the pace of development for many species, including humans (Arendt, 1997; Brown et al., 2004; Metcalfe and Monaghan, 2001; Pontzer et al., 2016). The interactions between food intake and development are complex and involve hormonal signaling (Bergland et al., 2008; Tang et al., 2011). Finally, cellular metabolism can alter the pace of development. For example, the evolutionarily conserved clk1 gene encodes a mitochondrial enzyme necessary for normal cellular respiration (Felkai et al., 1999), and loss of the clk1 gene in nematodes and mice results in developmental delays (Levavasseur et al., 2001; Nakai et al., 2001; Wong et al., 1995). In Drosophila, restricting glucose consumption by cells slows development (Brogiolo et al., 2001; Layalle et al., 2008; Rulifson et al., 2002; Shingleton et al., 2005). Gillooly et al. (2002) formulated a general quantitative model that relates developmental tempo to organismal mass, cellular metabolic rate, and temperature. Strikingly, the model fits meta-data spanning the major animal phyla, suggesting a universal relationship between metabolism and developmental tempo.

Many developmental processes involve specification of different cell types in a stereotyped sequence. All of these differentiated cell types originate from progenitor cells. The sequence of cell differentiation is driven by changes in the gene expression program within progenitors. Gene regulators, typically transcription factors, are sequentially activated and repressed, resulting in transient periods of increased activity. During these periods, they change gene expression in the progenitors. This coincides with and causes a temporal series of cell fate decisions. Because



¹Department of Molecular Biosciences, Northwestern University, Evanston, IL 60208, USA

²Department of Chemical and Biological Engineering, Northwestern University, Evanston, IL 60208, USA

³NSF-Simons Center for Quantitative Biology, Northwestern University, Evanston, IL 60208, USA

⁴Howard Hughes Medical Institute, California Institute of Technology, Pasadena, CA 91125, USA

⁵Northwestern Institute on Complex Systems, Northwestern University, Evanston, IL 60208, USA

⁶Department of Physics and Astronomy, Northwestern University, Evanston, IL 60208, USA

⁷These authors contributed equally

⁸Present address: Sg2/Vizient, Skokie, IL, USA

⁹Present address: Costello Medical, Cambridge, UK

¹⁰Lead Contact

^{*}Correspondence: amaral@northwestern.edu (L.A.N.A.), r-carthew@northwestern.edu (R.W.C.) https://doi.org/10.1016/j.cell.2019.06.023

these regulators frequently interact with one another, the entire cascade constitutes a gene regulatory network (GRN). Such GRNs have been characterized for embryogenesis (Cusanovich et al., 2018; Davidson and Erwin, 2006; Lawrence, 1992), development of the central nervous system (CNS) (Kohwi and Doe, 2013), and development of the sensory nervous system (Cepko, 2014). Because the tempo of development can vary, GRN dynamics must be able to reliably adjust to a variable timing mechanism. Therefore, understanding how these GRNs adapt to a variable timescale is crucial for understanding the mechanisms of animal development.

Phenomenological observations suggest that there are limits to the timescales to which development may adapt. Although broiler chickens have been successfully bred for rapid growth, frequent abnormalities in musculoskeletal development are evident in such breeds (Julian, 2005; Whitehead et al., 2003). Animals (and humans) experience hyper-normal growth rates when they initially experience delayed growth (Arendt, 1997). Such compensatory growth is linked to a variety of developmental and physiological defects (Metcalfe and Monaghan, 2001). Conversely, slowing growth can alleviate defects caused by mutations that impair development. As first noted by Morgan (1915, 1929), morphological phenotypes can be suppressed by limiting the nutrition of mutant animals (Child, 1939; Sang and Burnet, 1963). Likewise, raising animals under lowered temperatures can sometimes suppress the phenotypes of mutations that are not classical temperature sensitive (ts) alleles (Child, 1935; Krafka, 1920; Lewis et al., 1980; Villee, 1943). Collectively, these observations suggest that an unknown mechanism ensures successful developmental outcomes amidst variability in developmental tempo.

Here, we explored this mechanism. We find that impairing gene repression in GRNs only causes developmental errors when cell metabolism and growth rate are normal. When either energy metabolism or protein synthesis rate is reduced, developmental errors are reduced or even suppressed. We find that this relationship between metabolism and repression is so prevalent that the entire microRNA family becomes less essential for development when metabolism is slowed. Using a general mathematical modeling framework, we show that multiple layers of weak repression render gene expression dynamics independent of variable biochemical rates. When rates are modestly reduced, fewer repressors are needed to ensure normal expression dynamics. We experimentally validate this model prediction by following GRN dynamics in Drosophila. Our findings support a new mechanism whereby layers of gene repression allow development to proceed faster when metabolic conditions allow it. The need for flexible and robust developmental outcomes could provide an evolutionary impetus for the high prevalence of genetic redundancy.

RESULTS

Developmental patterns arise from directed dynamics of cell-cell signaling and gene regulation. The sensory organs of *Drosophila* are a classic system with which to study these phenomena (Quan and Hassan, 2005). A broad collection of gene mutations has specific effects on the formation of various sensory organs.

The affected genes encode transcription factors, microRNAs, signaling factors, and other gene regulators. We used such mutations to readdress the relationship between reduced metabolism and phenotype suppression that was first observed by Morgan (1915, 1929). We did so by scoring *Drosophila* sensory mutant phenotypes under conditions of reduced energy metabolism.

To reduce metabolism, we generated animals that had genetic ablation of their insulin-producing cells (IPCs) in the brain (Figure 1A). IPC ablation limits synthesis and release of insulin-like peptides (ILPs) and reduces the amount of glucose cells consume (Broughton et al., 2005; Rulifson et al., 2002). It also reduces the abundance of the mitochondrial ATP synthase enzyme complex in cells (Figure S1). Moreover, inhibition of ILP production reduces the whole-body metabolic rate of Drosophila, as measured by calorimetry (Zhang et al., 2009). IPC ablation results in 70% slower development (Figure 1B) and small but normally proportioned adults (Figure 1C) (Ikeya et al., 2002; Rulifson et al., 2002). Therefore, reduced ILP production by IPC ablation broadly decreases cellular energy metabolism and slows development.

Mutation of Repressors Has Less Effect When Metabolism Is Reduced

Yan is a transcription factor that maintains cells of the developing compound eye in a progenitor-like state (Graham et al., 2010). The protein is transiently expressed in cells (Peláez et al., 2015) and is cleared from differentiating photoreceptor (R) cells by multiple repressors acting on its transcription, mRNA stability, and protein stability (Figure S2A). The microRNA miR-7 represses post-transcriptional expression of Yan in the developing eye (Li and Carthew, 2005). When the mir-7 gene was specifically ablated in the compound eye of an otherwise wild-type animal, it resulted in small malformed adult eyes caused by errors in R cell differentiation (Figure 1D). This phenotype was highly penetrant in genetically mosaic animals (Figure 1E). However, when energy metabolism was slowed by IPC ablation, loss of mir-7 was much less important for the formation of correctly patterned eyes (Figure 1E). We also examined mutations affecting post-translational modification of Yan. The epidermal growth factor (EGF) and Sevenless (Sev) receptor tyrosine kinases activate MAP kinase in the progenitors of R7 photoreceptors (Figure S2A). MAP kinase phosphorylates Yan protein, leading to its ubiquitin-mediated degradation (Rebay and Rubin, 1995). This clearance of Yan protein enables differentiation of R7 cells (Voas and Rebay, 2004), and when sev is mutated, cells completely fail to differentiate as R7 photoreceptors (Figure 1F). However, slowing metabolism allowed a small but significant number of sev mutant cells to become R7 photoreceptors (Figure 1G). Importantly, because the sev mutant makes no protein products (Banerjee et al., 1987), rescue of the mutant phenotype was not simply due to more functional Sev protein molecules being present in slowly metabolizing cells.

We also examined mutations that affect formation of sensory bristles for evidence of metabolic interactions. The transcription factors Achaete, Scute, and Senseless (Sens) transiently appear in a cluster of proneural cells before they are upregulated in one cell, which differentiates into a sensory bristle (Jafar-Nejad et al.,

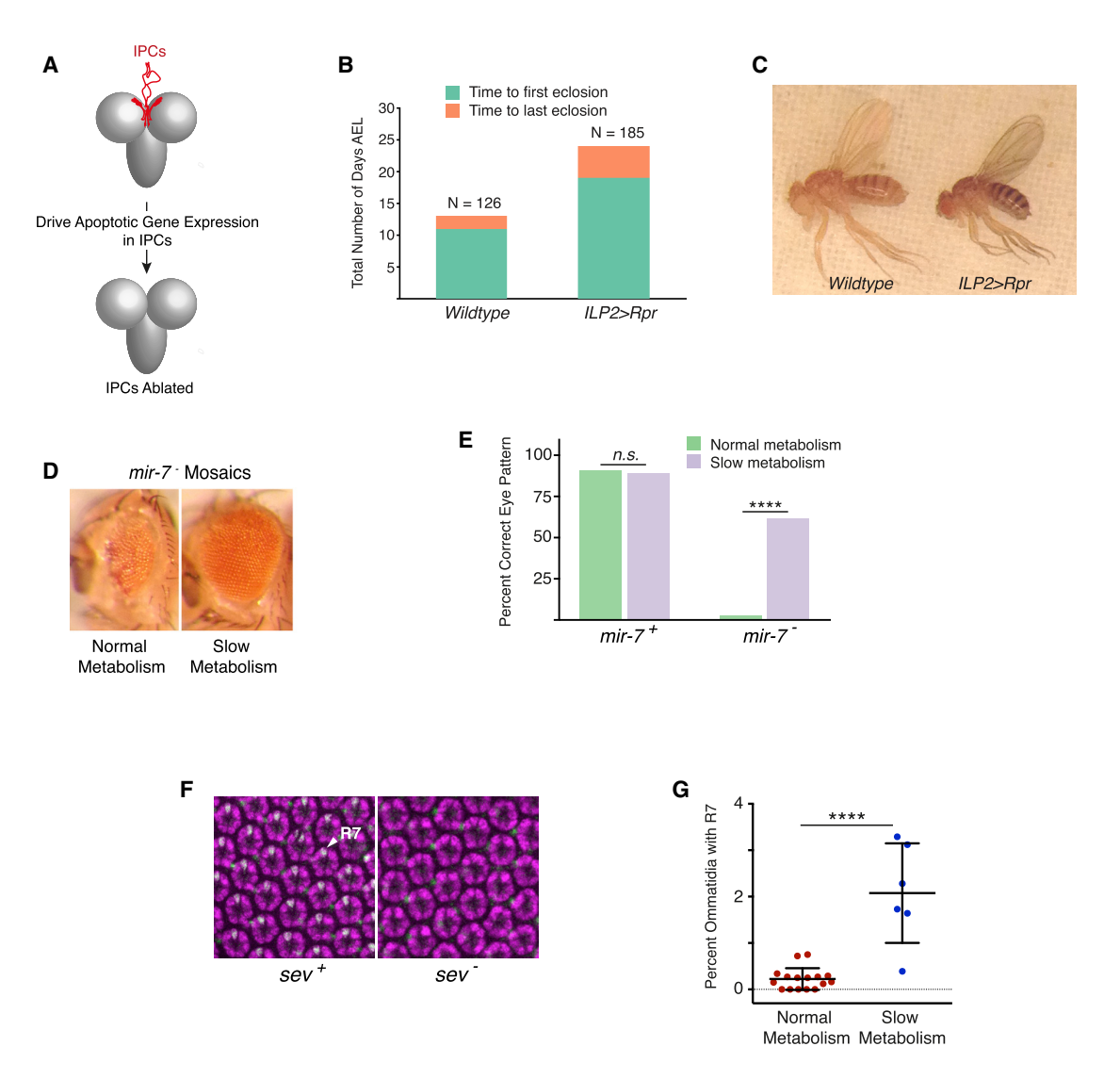


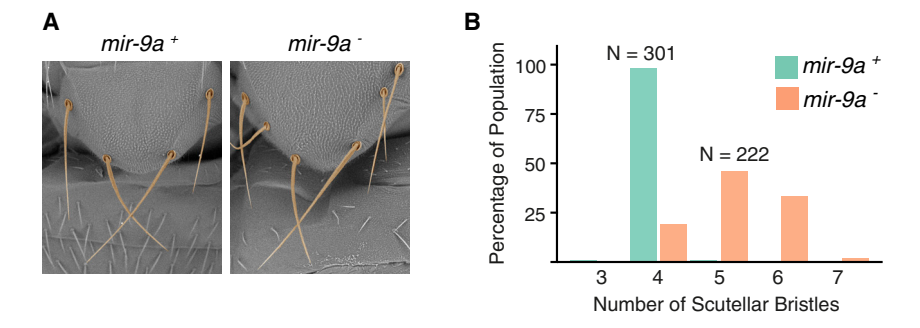
Figure 1. Eye Developmental Defects Are Rescued by Slower Energy Metabolism

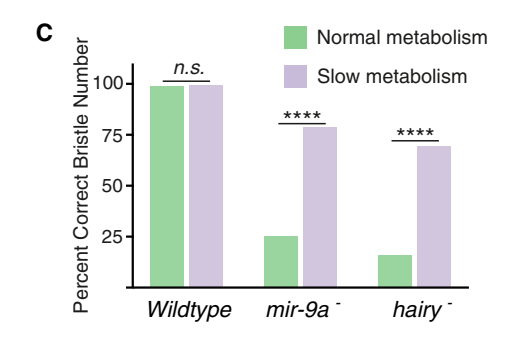
(A) Strategy to ablate IPCs (red) in the young fly brain. Gal4 expressed under control of the promoter for the Insulin-Like Peptide 2 (ILP2) gene drives production of the pro-apoptotic protein Reaper (Rpr) specifically in IPCs of the brain.

- (B) Number of days after egg laying (AEL) when the first individual in either wild-type or ILP2 > Rpr populations eclosed (hatched from pupa into adult) and the time when the last individual in each population eclosed.
- (C) The left adult female had its IPCs intact, whereas the right female had its IPCs ablated.
- (D) Genetically mosaic individuals with a mir-7+ body and a mir-7 mutant eye. The left individual with the mispatterned eye has its IPCs intact, whereas the right individual with a normally patterned eye has had its IPCs ablated.
- (E) Eye patterning is more normal when mosaic individuals metabolize slowly because of IPC ablation. The p values are from chi-square tests with Yates' correction.
- (F) Eye cells stained for markers so that R7 cells (white) can be distinguished from other R cells (purple) and bristle cells (green). Each ring of R cells is an ommatidium. Null mutation of sev results in no R7 cells (right).
- (G) IPC ablation increases the percentage of ommatidia that contain an R7 cell in sev mutants. Each data point represents one eye sample where between 481 and 837 ommatidia were scored. The p value is from a one-way ANOVA with Bonferroni correction.
- ****p < 0.0001; n.s., p > 0.05. See also Figures S1 and S2.

2003). They are downregulated in other cells within a proneural cluster, ensuring that just one bristle develops from each cluster (Figure S2B). microRNA miR-9a represses Sens protein expression, and mir-9a mutants frequently develop ectopic sensory bristles because this repression is missing (Figures 2A and 2B) (Cassidy et al., 2013; Li et al., 2006). However, when mir-9a mutants had their IPCs ablated, errors in bristle number were greatly reduced (Figure 2C).

The transcription factor Hairy directly represses transcription of the achaete and scute genes during selection of cells for bristle fates (Figure S2B) (Van Doren et al., 1994). Mutation of hairy causes some individuals to develop ectopic large bristles.







However, this effect of *hairy* mutation was strongly suppressed when energy metabolism was slowed (Figure 2C). We saw a similar effect on a *cis*-regulatory module (CRM) that represses transcription of the *wingless* (*wg*) gene (Figure S2B). The *Sternopleural* (*Sp-1*) mutation is present in a CRM located on the 3' flank of *wg* (Neumann and Cohen, 1996), causing *wg* misexpression and development of ectopic bristles (Figure 2D). However, the ectopic bristle phenotype of the *wg* ^{Sp-1} mutant was almost totally reversed under conditions of slowed energy metabolism (Figure 2D).

In conclusion, IPC ablation suppressed developmental phenotypes caused by mutations in genes that repress other genes at the transcriptional, post-transcriptional, and post-translational levels.

MicroRNAs Are Dispensable When Metabolism Is Reduced

The mutations examined so far affect diverse types of regulators, including microRNAs, transcription factors, and signaling molecules. However, all of the mutations have something in common:

Figure 2. Sensory Bristle Developmental Defects Are Rescued by Slower Energy Metabolism

(A) There are frequently more than four scutellar bristles in a *mir-9a* mutant.

(B) Distribution of scutellar bristle numbers in wildtype and *mir-9a* mutant populations. The distribution between wild-type and mutant is significantly different (p < 0.0001, Kolmogorov-Smirnov test).

(C) IPC ablation increases the proportion of *mir-9a* and *hairy* mutants that have the wild-type number of scutellar bristles. ****p < 0.0001; n.s., p > 0.05.

(D) Under normal conditions, wg^{Sp-1} flies have more than the wild-type three sternopleural bristles. IPC ablation causes most wg^{Sp-1} individuals to have three bristles. Shown is the number of individuals scored with the phenotype versus the total number of scored individuals. IPC ablation suppresses the ectopic bristle phenotype (p < 0.0001, Fisher's exact test)

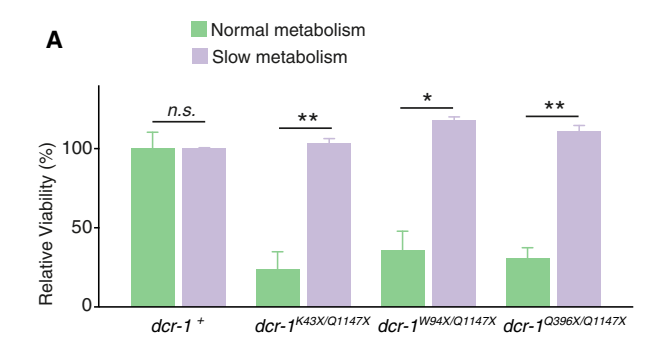
See also Figure S2.

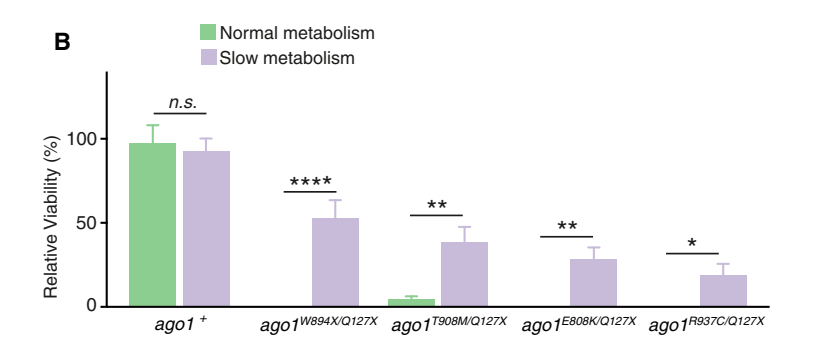
they affect repressive interactions between genes. To survey the depth of this relationship between gene repression and metabolism, we eliminated an entire family of regulatory repressors that control all stages of Drosophila development. The microRNA family is composed of 466 distinct microRNAs in Drosophila melanogaster (Kozomara and Griffiths-Jones, 2014). Virtually all microRNAs require Dicer-1 (Dcr-1) protein for their proper biosynthesis and Ago1 protein as a partner to repress target gene expression (Carthew and Sontheimer, 2009). Protein-null mutations in either the dcr-1 or ago1 gene are organismal lethal and abolish microRNA-mediated gene repres-

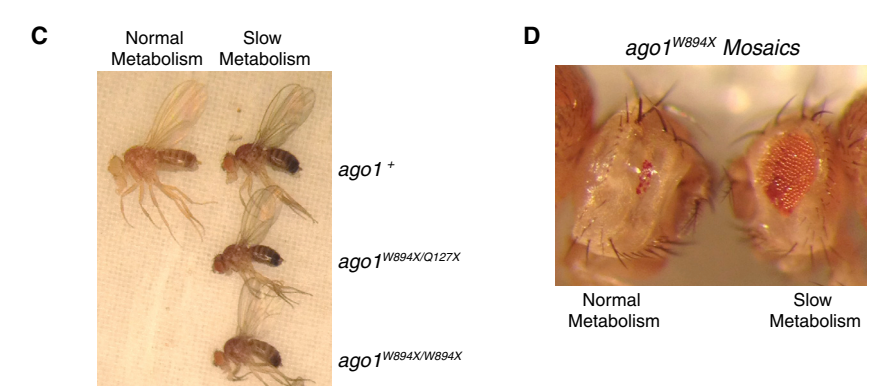
sion (Pressman et al., 2012). We raised different null *dcr-1* mutants under conditions of slower energy metabolism and found that many more animals survived development (Figure 3A). *Ago1*-null mutants are 100% embryonic lethal, but mutant lethality was suppressed when animals metabolize slowly because of IPC ablation (Figure 3B). The mutants survived to adulthood, and most survivors had normal eye and bristle patterns as well as other body structures, indicating rescue of a massive array of developmental defects (Figure 3C). Rescue could also be seen when Ago1 was specifically ablated in cells of the compound eye; eye development was strongly rescued by slower energy metabolism (Figure 3D). Therefore, a major class of regulatory repressors is rendered less essential for development when energy metabolism is slowed.

A Dynamical Model Describes the Relationship between Metabolism and Developmental Error Frequency after Repressor Loss

We turned to computational modeling to elucidate the mechanism linking gene repression, developmental phenotypes, and







metabolism. Because this relationship affects many GRNs during many stages of development, we sought to directly model the emergent dynamics of these systems rather than the specific regulatory interactions behind them.

Our modeling framework is premised on the progressive restriction of cell fate potential as development proceeds. Cell fate transitions are coordinated by the sequential activities of one or more genes whose products are synthesized, act, and are then eliminated until they are needed later in other cells. Viewed collectively, the resultant dynamics resemble a cascade of transient pulses of protein expression (Figure 4A). When expression of a gene is induced by a stimulus (the input), its timely attenuation ensures that protein expression remains transient (Figure 4B). GRNs often have multiple layers of repressive feedback to attenuate expression of these genes. To model

Figure 3. The MicroRNA Family Is Less Essential When Energy Metabolism Is Slowed

- (A) Pupal viability of various *dcr-1* nonsense mutants is fully rescued when IPCs are ablated.
- (B) Adult viability of various ago1 missense and nonsense mutants is rescued when IPCs are ablated.
- (C) Representative *ago1* adults with normal or slowed metabolism.
- (D) Genetically mosaic individuals with $ago1^+$ bodies and $ago1^{WB94X}$ mutant eyes. Left, a representative individual with normal metabolism has almost no eye tissue (24 of 24 animals). Right, a representative individual with slowed metabolism has rescued eye tissue. Of 70 such animals, 46 had this phenotype, 20 had normal eyes, and 4 had eyes that resembled the left animal. This is a significant difference; p < 0.0001, chi-square test with Yates' correction.

Error bars, SD. ****p < 0.0001; **p < 0.01; *p < 0.05; n.s., p > 0.05.

these dynamical features of developmental gene expression, we chose a subfield of mathematics known as control theory because it is a general theory describing feedback systems.

In our control theory model, a transient stimulus activates expression of a regulatory gene, whose protein is the output (Figures 4C and S3A). Acting in parallel, one or more feedback control elements detect the increase in protein level and act to downregulate it at the level of gene transcription, mRNA stability, or protein stability. These control elements can be thought of as independent repressors working in parallel to bring the protein level back to a basal steady state (Figure 4D). Because gene expression is noisy (Arias and Hayward, 2006), we also incorporated intrinsic noise into the model. When we ran model simulations, protein expression followed

a biphasic trajectory in each simulation (Figure 4E, dotted line). However, each simulation gave a slightly different trajectory because of expression noise; therefore, we performed thousands of simulations to capture the distribution of trajectories (Figure 4E).

Because each pulse must keep pace with parallel steps in the program, successful development is contingent upon timely attenuation of the output. We defined a lower threshold that the output level must cross before a subsequent fate change is triggered (Figure 4E). Simulated trajectories that fail to reach the threshold in time constitute errors (Figure 4F). Notably, errors become more frequent when one repressor is lost (Figures 4E–4G). This property is observed over a broad range of model parameter values, regardless of the value at which the threshold is defined and regardless of whether repressors act

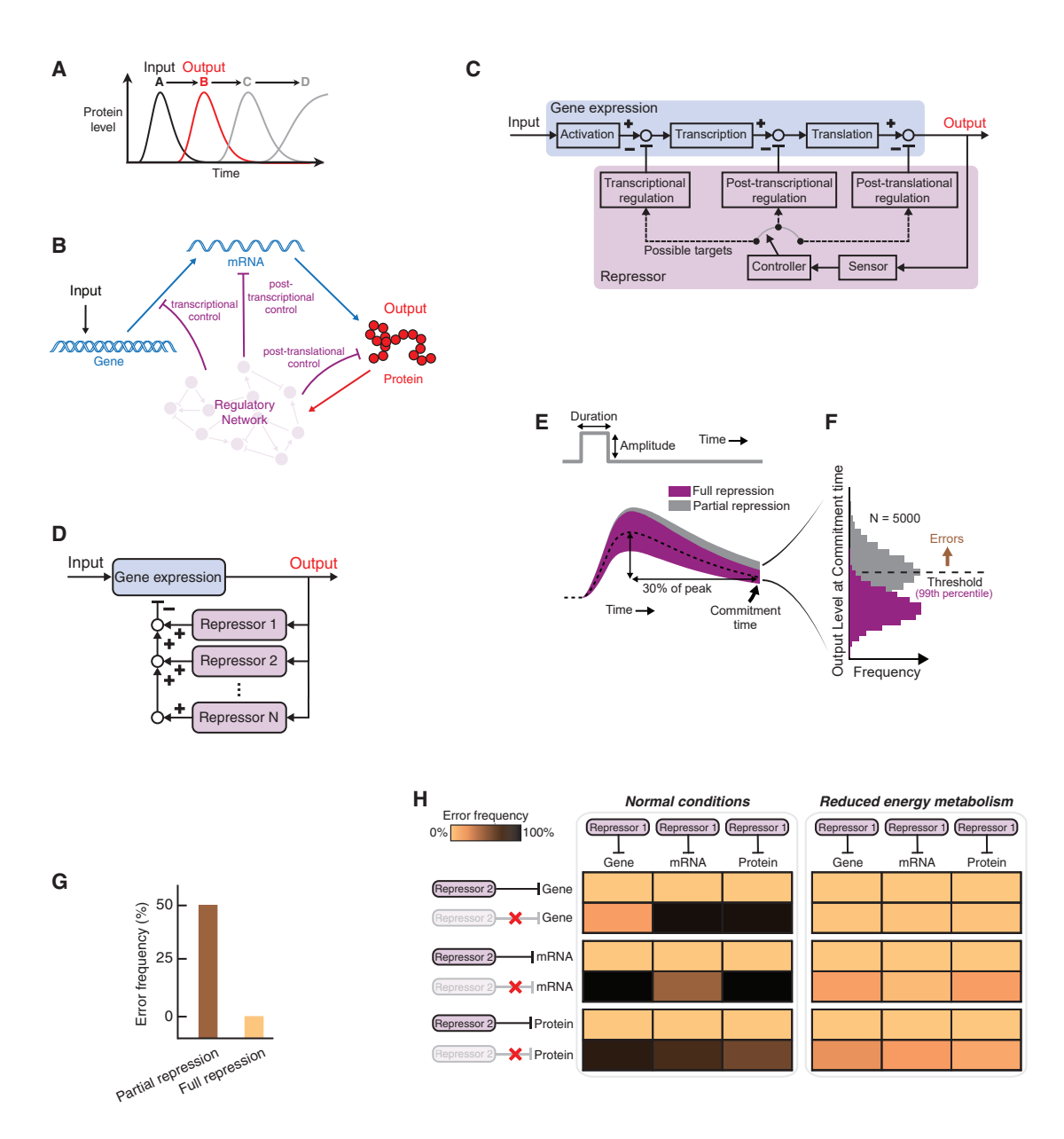
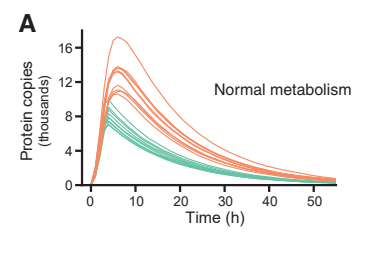
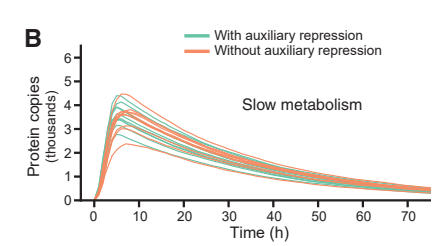


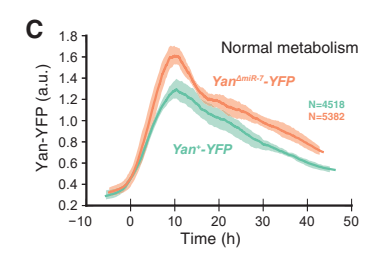
Figure 4. Modeling Gene Expression Dynamics during Development

(A) A program of gene expression occurs as a cell passes through a series of developmental states. The model focuses on transient expression of a single gene within the cascade.

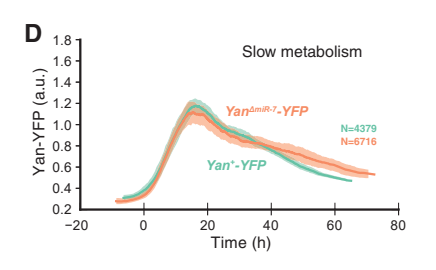
- (B) Gene expression in response to a transient input stimulus. Protein output is subject to layers of repression acting at the gene, transcript, and protein levels.
- (C) Control representation of a single feedback loop as depicted in (B). Arrows represent biochemical information transfer, and boxes represent the processes that relate these signals. Open circles indicate logical summation points, and closed circles indicate exclusive switches.
- (D) Gene expression may be regulated by multiple repressors acting in parallel.
- (E) Model simulations showing protein output over time. Input is shown at top. Shown below are 98% of the 5,000 simulated output trajectories, which merge together into a band of trajectories. Grey and purple denote simulations with one and two post-translational repressors, respectively. The dotted line indicates the mean trajectory with full repression. Commitment time is defined as the time needed for the dotted line to reach 30% of its peak value. The threshold is set at the upper boundary of the full repression confidence band at the commitment time.
- (F) With partial repression, fewer simulations cross the threshold within the commitment time. Each failure to cross the threshold in time is an error.
- (G) Error frequency is greater with partial post-translational repression.
- (H) Errors become more frequent with partial repression (left) regardless of how repressors act on gene expression. However, partial repression imparts very few errors when ATP-dependent parameter values are reduced by 50% (right). See also Figures S3 and S4.







See also Figure S5.



(C) Yan-YFP dynamics for wild-type Yan-YFP and mutant Yan-4miR-7-YFP genes under normal metabolic conditions. (D) Yan-YFP dynamics for wild-type and mutant genes when the IPCs have been ablated.

Figure 5. Expression Dynamics Are Resistant to Repressor Loss When Energy Metabolism Is Reduced

(A and B) Simulated protein output under the control of an auxiliary post-transcriptional repressor (green) and when the repressor is removed (orange). All simulations (green and orange) are also under control of a constitutive repressor. Shown are ten randomly chosen samples from a total population of 5,000 trajectories for each condition.

- (A) Simulations performed with normal ATP-dependent reaction rates
- (B) Simulations performed following a 50% reduction in the rate of ATP-dependent reactions.
- (C and D) Yan-YFP protein dynamics in eye disc progenitor cells. Time 0 marks the time when Yan-YFP induction occurs. Solid lines represent moving averages. Shaded regions denote 95% confidence intervals. Each line average is calculated from a composite of measurements of between 4,379 and 6.716 cells

transcriptionally, post-transcriptionally, or post-translationally (Figures S3B and 3C).

The modeling framework allowed us to ask whether multiple layers of repression are less important for developmental outcome when energy metabolism is reduced. To answer this question, we halved the rate parameters of each ATP-utilizing reaction to reflect conditions of reduced energy metabolism. Although ATP content remains fairly constant in cells facing limited respiration, the flux of ATP synthesis and turnover is affected, manifesting as altered ratios of ATP to ADP and free phosphate (Brown, 1992). Anabolic processes are highly dependent on the ATP:ADP ratio (Atkinson, 1977). When we halved ATP-dependent rate parameters, we observed that error frequency in developmental outcome did not increase when a repressor was lost (Figure 4H). This insensitivity to repressor loss persisted whether repression was transcriptional, post-transcriptional, or post-translational. The effect was observed across a wide range of parameter values (Figures S4A and S4B), irrespective of where the threshold was set (Figure S4C) and regardless of whether a basal stimulus was present (Figure S4D). In many cases, the effect remained modestly apparent when the stimulus duration was extended to maintain comparable protein levels under conditions of reduced energy metabolism (Figure S4E). Thus, the model indicates that the frequency of developmental errors is generally less sensitive to changes in repression when energy metabolism is reduced.

Our modeling framework promotes simplicity at the expense of two notable limitations. First, gene expression models frequently utilize cooperative kinetics to reproduce the nonlinearities and thresholds encountered in transcriptional regulation. Second, the number of transcriptionally active sites within a cell is limited by gene copy number. We modified the framework to implement each of these complexities and found that error frequencies remained broadly suppressed when ATP-dependent rate parameters were reduced (Figures S4F and S4G). We also considered whether reduced glucose consumption by cells

might hinder the synthesis of nucleotide and amino acid precursors required for RNA and protein synthesis. Constraining these synthesis rates also suppressed the rise in error frequency when a repressor was lost (Figure S4H).

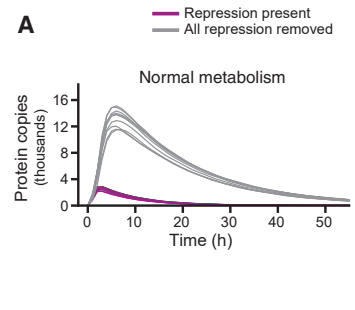
Combined, all of these simulations suggest that phenotype suppression may arise from the differential effects of repressor loss on gene expression dynamics.

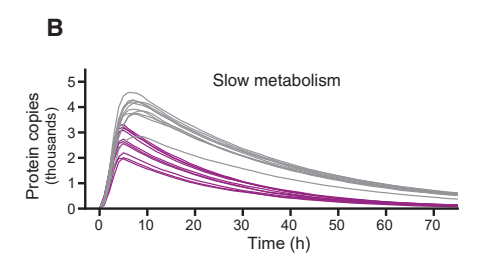
Experimental Validation of the Dynamic Model

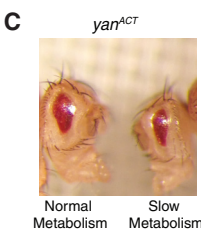
Our simulations make a general prediction as to how protein expression dynamics change when a repressor is lost; pulse amplitude and duration both increase, yielding elevated protein levels across the time course (Figure 4E). We quantified the change in expression dynamics by constructing a confidence band around the set of trajectories simulated with full repression (Figure S5A). We then evaluated the fraction of trajectories simulated with partial repression that exceed the confidence band (Figure S5B) and confirmed that protein levels generally increase when a repressor is removed. This effect is highly robust to parameter variation for all types of repressors (Figure S5C). For example, when a post-transcriptional repressor akin to a micro-RNA is removed, 78% of simulation trajectories are elevated across the time course (Figure 5A).

We then halved the model's ATP-dependent parameters, ran simulations, and compared trajectories with full or partial repression. Strikingly, there was little difference between the trajectories with full repression versus loss of a post-transcriptional repressor (Figure 5B). Only 16% of trajectories exceeded the confidence band, and this was robust to extensive parameter variation (Figure S5D). These results led us to predict that expression dynamics will be much less sensitive to loss of a post-transcriptional repressor when we reduce energy metabolism.

We experimentally tested this key prediction by measuring the expression dynamics of the regulatory protein Yan. Yan exhibits pulsatile dynamics in the larval eye, where its expression is







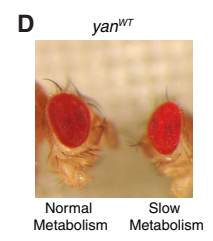


Figure 6. Reduced Energy Metabolism Cannot Compensate for Complete Loss of Repression

(A and B) Simulated expression of protein output with (purple) and without (gray) any repression of the target gene. Shown are ten randomly chosen samples from a total population of 5,000 trajectories for each condition. Error frequencies exceed 99% irrespective of metabolic conditions.

- (A) Simulations performed under normal conditions. (B) Simulations performed following a 50% reduction in the rate of ATP-dependent reactions.
- (C) Loss of eye tissue in a yan^{ACT} mutant is not suppressed by slower metabolism. Representative individuals were taken from N > 100 individuals for each condition.
- (D) Eye patterning in a yan^{WT} control is not affected by slower metabolism. Representative individuals were taken from N > 100 individuals for each

induced by a morphogenetic furrow that traverses the eye disc. Eye cells located in the morphogenetic furrow rapidly upregulate Yan protein abundance, as quantified by a YFP-tagged version (Peláez et al., 2015). Yan levels then gradually decay back to initial conditions in these cells. We compared Yan-YFP dynamics in eye disc cells from normal metabolizing larvae and larvae with ablated IPCs (Figures 5C and 5D). The same pulsatile dynamics were observed in both, but the amplitude of the pulse was slightly reduced and the duration was extended when metabolism was slower.

Yan expression is repressed by the microRNA miR-7 in the eye disc (Li and Carthew, 2005). There are four binding sites for miR-7 in the 3′ UTR of yan mRNA, and their mutation causes de-repression of Yan output. We eliminated miR-7 repression of Yan-YFP by mutating the four binding sites in the 3′ UTR of Yan-YFP mRNA to make Yan∆miR-7-YFP. In normal metabolizing eye cells, Yan-YFP protein made from the mutated gene pulsed with greater amplitude and showed impaired decay compared with Yan-YFP made from the wild-type gene (Figure 5C). These dynamics validate the first prediction made by our model (Figure 5A).

However, when metabolism was slowed, loss of miR-7 regulation had little to no effect on Yan expression. In animals with IPC ablation, Yan-YFP made from the mutated gene showed similar dynamics as Yan-YFP made from the wild-type gene (Figure 5D). This behavior clearly resembled the simulated dynamics under conditions of reduced energy metabolism (Figure 5B), validating the model's second prediction.

Loss of Full Repression and No Suppression of the Mutant Phenotype

Our modeling framework explains why mutant phenotypes are suppressed when metabolic conditions are reduced, prompting us to ask whether repression is needed at all under such conditions. We studied a model with a full complement of repressors and compared the results with a scenario in which all repressors were removed (Figure 6A). Error frequencies approached 100%

under normal metabolic conditions. Although expression dynamics were visibly less affected by repressor loss when ATP-dependent parameters were reduced, the error frequency remained very high (Figure 6B). Thus, the model predicts that there are limits to the severity of perturbations for which reductions in energy metabolism can compensate, and reducing energy metabolism does not eliminate the need for gene repression altogether.

To test this prediction, we expressed, in the eye, a *Yan* mutant transgene that is insensitive to all known repression of *yan* transcription, mRNA stability, and protein stability (Rebay and Rubin, 1995). The *Yan*^{Act} mutant adults had severely disrupted compound eye patterning (Figure 6C). This mutant eye phenotype was not suppressed by IPC ablation. Wild-type *Yan* transgenic adults with normal eye patterning were also unaffected (Figure 6D).

Limiting Protein Synthesis Reduces the Need for Repressors

Other aspects of metabolism can be used to explore coupling of developmental dynamics to time. In particular, protein synthesis is an important determinant of rates of growth and development (Lempiäinen and Shore, 2009). We used our modeling framework to investigate the effect of a 2-fold reduction in overall protein synthesis rate on the loss of a repressor. Our simulations generally predicted that gene expression dynamics would be less affected and that fewer developmental errors would occur (Figure 7A; Figures S6A–S6G).

We tested these predictions by using loss-of-function mutations in genes encoding various ribosomal proteins (RPs). These mutations cause the "Minute" syndrome of dominant, haploin-sufficient phenotypes, including slower growth and development (Marygold et al., 2007; Saebøe-Larssen et al., 1998). A total of 64 RP genes exhibit a Minute syndrome when mutated. As might be expected, a RP heterozygous mutant reduces the translational output of cells (Boring et al., 1989). RP mutants do so by signaling through the Xrp1 transcription factor to

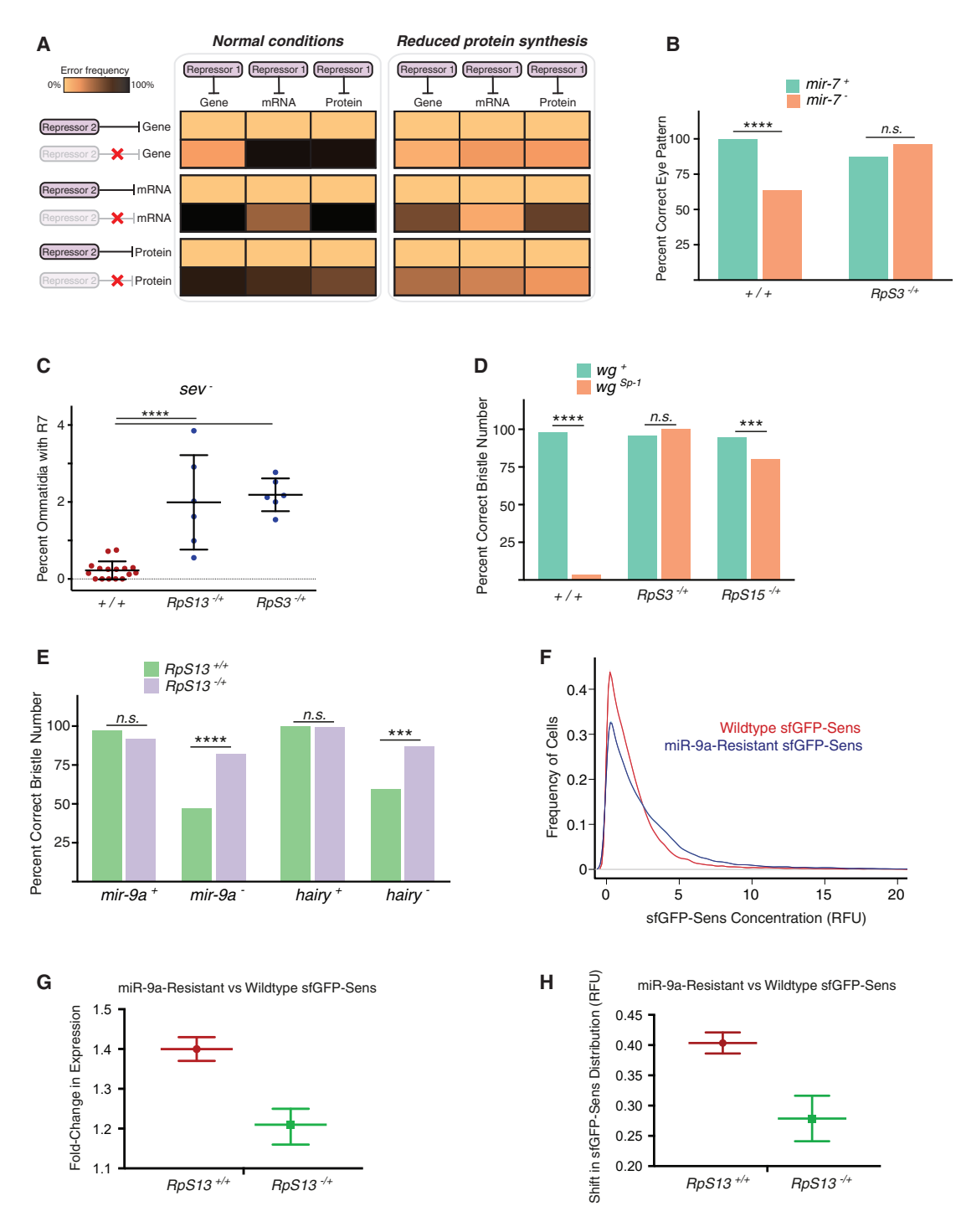


Figure 7. Reducing Protein Synthesis Rate Rescues Loss of Repressors on Sensory Organ Development and Expression Dynamics

(A) The model predicts increased frequency of error with partial repression regardless of how auxiliary repressors act on gene expression (left). However, partial repression induces fewer errors when protein synthesis-dependent parameter values are reduced by 50% (right).

(B) Loss of mir-7 does not cause adult eye mispatterning when RpS3 is heterozygous mutant.

(C) sev mutants have more R7-positive ommatidia when either RpS3 or RpS13 are heterozygous mutant. Each data point represents one eye sample, and between 481 and 837 ommatidia were scored for R7 cells within each eye sample.

(D) wg^{Sp-1} heterozygous individuals that are also heterozygous mutant for different RpS genes have sternopleural bristle numbers more similar to the wild type. (E) Developmental accuracy is recovered for both mir-9a and hairy mutants that are also heterozygous mutant for RpS13.

(legend continued on next page)

globally downregulate the protein synthesis rate (Lee et al., 2018a). We combined a subset of heterozygous *RP* mutants with the repressor mutations we had studied previously. As predicted, the *RP* mutants suppressed the developmental phenotypes of mutations in *wg*, *mir-7*, *sev*, *hairy*, and *mir-9a* (Figures 7B–7E).

We also tested the prediction that expression dynamics would be less affected by repressor loss when protein synthesis was reduced. The Sens protein is transiently expressed in proneural cells during selection of sensory bristle fates in the imaginal wing disc (Nolo et al., 2000). Bordering the presumptive wing margin, stripes of proneural cells express Sens protein over a spectrum of levels, reflecting heterogeneity in Wg and Notch regulation of its expression (Jafar-Nejad et al., 2006; Quan and Hassan, 2005). miR-9a weakly represses sens expression in these cells (Li et al., 2006). We recombineered a 19-kb sens transgene, tagged N-terminally with superfold GFP (sfGFP), that functionally replaced the endogenous sens gene (Cassidy et al., 2013; Venken et al., 2006). Quantitative measurement of sfGFP fluorescence in individual proneural cells yielded the expected distribution of sens expression (Figure 7F). We compared this distribution with one derived from individuals expressing a mutated sfGFP-sens transgene in which its miR-9a binding sites had been mutated (Cassidy et al., 2013). Mutation of the miR-9a binding sites in sfGFP-sens shifted the fluorescence distribution (Figure 7F) and resulted in an average 1.4-fold increase in sfGFP-Sens levels (Figure 7G). We then tested the effects of miR-9a on sfGFP-sens expression when an RP gene was heterozygous mutant. As predicted (Figure S6B), loss of miR-9a regulation had less effect on sfGFP-Sens protein levels in the RP mutant (Figures 7G and 7H).

DISCUSSION

Growth and development are fueled by metabolism. This means that the tempo of development depends on metabolic rate. Thus, the dynamics of developmental gene expression must faithfully adjust to a variable timescale. We have shown that multi-layered weak repression within GRNs plays an unexpected function in synchronizing gene expression dynamics with the variable pace of the developmental program. Multiple repressors are required for accelerated development when metabolism is high, and they become functionally redundant when metabolism is low. Multiple repressors therefore allow reliable development across a broader range of metabolic conditions than tolerated otherwise.

Our model explains long-standing observations linking nutrient limitation to suppression of mutant phenotypes (Morgan, 1915, 1929). Presumably, such mutations cripple regulatory

genes acting on developmental GRNs. Our model might also offer an explanation for why animals that undergo above-normal growth exhibit compromised development (Arendt, 1997; Metcalfe and Monaghan, 2001). Wild-type GRNs might function across a limited range of metabolism, with functionality breaking down when metabolism exceeds that range.

Another mechanism to explain phenotype suppression relies on a steady-state and not dynamic perspective of gene expression. Genome-wide gene expression patterns could conceivably change with organismal growth rate. This is the case for chemostat-grown yeast cells, where the expression of 27% of all genes correlates with growth rate (Brauer et al., 2008). Most genes associated with stress response are overexpressed when cells grow at a slow rate (Brauer et al., 2008; Lu et al., 2009). Such stressresponsive expression could modulate global processes such as protein folding and turnover, among others, and attenuate phenotypes when metabolism is slowed (Webb and Brunet, 2014). Indeed, molecular chaperones have been found to affect the penetrance of diverse gene mutations in C. elegans and Drosophila (Casanueva et al., 2012; Rutherford and Lindquist, 1998). However, this steady-state model does not explain why gene expression dynamics are conditionally dependent on the availability of repressors. We found that repression of Yan and Sens expression by microRNAs becomes more redundant when metabolic rates are slowed. Nevertheless, phenotype suppression might be due to a combination of mechanisms, including steady-state stress response and gene expression dynamics.

Our varied analyses suggest that the relationship between metabolism and gene expression dynamics is widespread. We found that the entire family of 466 microRNAs in *Drosophila melanogaster* become much less essential for development when energy metabolism is slowed. The extensive literature on microRNA function in *Drosophila* implicates them in practically all facets of the fruit fly's life (Bushati and Cohen, 2007; Carthew et al., 2017). Various explanations have been provided for why this family of weak repressors has flourished in the animal kingdom, chief among them the idea that they act as buffers for gene expression (Ebert and Sharp, 2012). We now posit that microRNAs also provide a robust means for developmental processes to accommodate fluctuations in metabolism.

Raising animals at lower temperatures can suppress the phenotypes of mutations that are not classical ts alleles (Child, 1935; Krafka, 1920; Lewis et al., 1980; Villee, 1943). Indeed, loss of sens repression by miR-9a has less impact on bristle development when temperature is lowered (Cassidy et al., 2013). Because metabolic rate varies with temperature (Zuo et al., 2012), it is possible that temperature-dependent phenotype suppression may also be attributed to a relaxed requirement for coupling gene expression dynamics to a metabolism-dependent timescale. We

⁽F) Frequency distribution of the sfGFP-Sens protein level in cells bordering the wing margin of white prepupal wing discs. Shown are distributions of cells expressing either wild-type sfGFP-sens or sfGFP-sens in which miR-9a binding sites have been mutated. Shaded regions denote 95% confidence intervals. Each line is calculated from a composite of measurements of more than 18,000 cells.

⁽G) The fold change in median sfGFP-sens expression caused by miR-9a binding site mutations. Measurements were taken in RpS13 wild-type and heterozygous mutant backgrounds. Shown are 99% confidence intervals for the estimated fold change.

⁽H) The shift in the fluorescence distribution of sfGFP-Sens-positive cells caused by miR-9a binding site mutations, as determined by a Mann-Whitney-Wilcoxon test. The upward shift is smaller in an *RpS13* heterozygous mutant background. Shown are 95% confidence intervals for the shift.

(B–E) Error bars, SD. ****p < 0.0001; ***p < 0.001; n.s., p > 0.05. See also Figure S6.

explored this notion using our modeling framework, and the results are inconclusive (S.M.B., N.B., and L.A.N.A., unpublished data). We anticipate that error suppression will be weak when temperature-modulated expression dynamics are the sole cause. This is because temperature should affect the rates of both anabolic and catabolic processes involved in gene expression. In contrast, limiting ATP availability or protein translation reduces the rates of anabolic reactions but not all catabolic reactions. This asymmetric effect on different steps in gene expression is a major reason why gene repression becomes less important when ATP availability or protein translation is limited.

Metabolic conditions drive variation of the intrinsic developmental tempo of each species. We have shown that layered weak repression within GRNs enables these fluctuations to occur without causing developmental errors. Metabolic conditions change in both space and time. Perhaps the selective advantage of a reliable developmental outcome amidst variable environmental conditions is a driving force in the evolution of gene regulatory networks.

STAR*METHODS

Detailed methods are provided in the online version of this paper and include the following:

- KEY RESOURCES TABLE
- LEAD CONTACT AND MATERIALS AVAILABILITY
- EXPERIMENTAL MODEL AND SUBJECT DETAILS
 - Drosophila Growth and Genetics
 - Transgenesis
- METHOD DETAILS
 - O R7 Cell Analysis in the Eye
 - Relative Viability
 - Eye Mispatterning
 - Bristle Scoring
 - O Quantification of sfGFP-Sens Expression in the Wing Disc
 - O Quantification of Yan-YFP Expression Dynamics in the Eye
 - ATP Synthase Immunofluorescence
 - Mathematical Modeling
 - Dependence of Model Parameters on Metabolic Conditions
 - Model Simulations
 - O Evaluation of Error Frequencies and Changes in **Expression Dynamics**
 - Parameter Variation and Sensitivity to Model Assumptions
 - Alternate Models
- QUANTIFICATION AND STATISTICAL ANALYSIS
- DATA AND CODE AVAILABILITY
 - Data Availability
 - Code Availability

SUPPLEMENTAL INFORMATION

Supplemental Information can be found online at https://doi.org/10.1016/j. cell.2019.06.023.

ACKNOWLEDGMENTS

We thank Jon Braverman for discussions and insights and the Bloomington Drosophila Stock Center and the Developmental Studies Hybridoma Bank for reagents. We also thank Alec Victorsen and Jennifer Moran for help with yan transgene recombineering and Diana Posadas and Hemanth Potluri for help with sens transgene recombineering. Jessica Hornick and the Biological Imaging Facility are acknowledged. We acknowledge support from the Chicago Biomedical Consortium (to J.J.C. and N.P.), the Malkin Foundation and Rappaport Foundation (to J.J.C.), the Northwestern Data Science Initiative (to R.G.), a John and Leslie McQuown gift (to L.A.N.A.), the NSF (1764421 to L.A.N.A., N.B., and R.W.C.), the Simons Foundation (597491 to L.A.N.A., N.B., and R.W.C), and the NIH (T32 GM008061 to J.J.C. and B.E., T32 CA080621 to R.B., and P50 GM81892 and R35 GM118144 to R.W.C.).

AUTHOR CONTRIBUTIONS

The experimental work was conceived by J.J.C. and R.W.C. The genetic experiments classifying phenotypes were performed by J.J.C., B.E., and A.B. under the supervision of R.W.C. N.P. designed and built the $Yan-YFP^{\triangle miR-7}$ mutant line, and R.B. performed imaging and analysis of Yan-YFP expression with assistance from S.M.B. and under the guidance of R.W.C. R.G. built the sfGFP-sens wild-type and mutant stocks with RpS13 and performed all imaging and analysis of sfGFP-Sens expression. The modeling was conceived by S.M.B., N.B., and L.A.N.A. All model analyses were performed by S.M.B. under the supervision of N.B. and L.A.N.A. The manuscript was written by S.M.B. and R.W.C. with input from all authors.

DECLARATION OF INTERESTS

The authors declare no competing interests.

Received: February 13, 2019 Revised: May 6, 2019 Accepted: June 12, 2019 Published: July 25, 2019

REFERENCES

Arendt, J.D. (1997). Adaptive intrinsic growth rates: An integration across taxa. Q. Rev. Biol. 72, 149-177.

Arias, A.M., and Hayward, P. (2006). Filtering transcriptional noise during development: concepts and mechanisms. Nat. Rev. Genet. 7, 34-44.

Arrowsmith, D.K., and Place, C.M. (1992). The linearization theorem. In Dynamical Systems: Differential Equations, Maps, and Chaotic Behaviour (Chapman & Hall), pp. 77-81.

Atkinson, D.E. (1977). Cellular Energy Metabolism and Its Regulation (Academic Press).

Atlas, M. (1935). The effect of temperature on the development of Rana pipiens. Physiol. Zool. 8, 290-310.

Banerjee, U., Renfranz, P.J., Hinton, D.R., Rabin, B.A., and Benzer, S. (1987). The sevenless+ protein is expressed apically in cell membranes of developing Drosophila retina; it is not restricted to cell R7. Cell 51, 151-158.

Bergland, A.O., Genissel, A., Nuzhdin, S.V., and Tatar, M. (2008). Quantitative trait loci affecting phenotypic plasticity and the allometric relationship of ovariole number and thorax length in Drosophila melanogaster. Genetics 180,

Boring, L.F., Sinervo, B., and Schubiger, G. (1989). Experimental phenocopy of a Minute maternal-effect mutation alters blastoderm determination in embryos of Drosophila melanogaster. Dev. Biol. 132, 343-354.

Brauer, M.J., Huttenhower, C., Airoldi, E.M., Rosenstein, R., Matese, J.C., Gresham, D., Boer, V.M., Troyanskaya, O.G., and Botstein, D. (2008). Coordination of growth rate, cell cycle, stress response, and metabolic activity in yeast. Mol. Biol. Cell 19, 352-367.

Brogiolo, W., Stocker, H., Ikeya, T., Rintelen, F., Fernandez, R., and Hafen, E. (2001). An evolutionarily conserved function of the *Drosophila* insulin receptor and insulin-like peptides in growth control. Curr. Biol. *11*, 213–221.

Broughton, S.J., Piper, M.D., Ikeya, T., Bass, T.M., Jacobson, J., Driege, Y., Martinez, P., Hafen, E., Withers, D.J., Leevers, S.J., and Partridge, L. (2005). Longer lifespan, altered metabolism, and stress resistance in *Drosophila* from ablation of cells making insulin-like ligands. Proc. Natl. Acad. Sci. USA 102, 3105–3110.

Brown, G.C. (1992). Control of respiration and ATP synthesis in mammalian mitochondria and cells. Biochem. J. 284, 1–13.

Brown, J.H., Gillooly, J.F., Allen, A.P., Savage, V.N., and West, G.B. (2004). Toward a metabolic theory of ecology. Ecology *85*, 1771–1789.

Bushati, N., and Cohen, S.M. (2007). microRNA functions. Annu. Rev. Cell Dev. Biol. 23, 175–205.

Carthew, R.W., and Sontheimer, E.J. (2009). Origins and mechanisms of miRNAs and siRNAs. Cell *136*, 642–655.

Carthew, R.W., Agbu, P., and Giri, R. (2017). MicroRNA function in *Drosophila melanogaster*. Semin. Cell Dev. Biol. 65, 29–37.

Casanueva, M.O., Burga, A., and Lehner, B. (2012). Fitness trade-offs and environmentally induced mutation buffering in isogenic *C. elegans*. Science 335. 82–85.

Cassidy, J.J., Jha, A.R., Posadas, D.M., Giri, R., Venken, K.J.T., Ji, J., Jiang, H., Bellen, H.J., White, K.P., and Carthew, R.W. (2013). miR-9a minimizes the phenotypic impact of genomic diversity by buffering a transcription factor. Cell *155*, 1556–1567.

Cepko, C. (2014). Intrinsically different retinal progenitor cells produce specific types of progeny. Nat. Rev. Neurosci. 15, 615–627.

Child, G. (1935). Phenogenetic studies on *scute-1* of *Drosophila melanogaster*. I. The associations between the bristles and the effects of genetic modifiers and temperature. Genetics *20*, 109–126.

Child, G. (1939). The effect of increasing time of development at constant temperature on the wing size of *vestigial* of *Drosophila melanogaster*. Biol. Bull. 77, 432–442

Cusanovich, D.A., Reddington, J.P., Garfield, D.A., Daza, R.M., Aghamirzaie, D., Marco-Ferreres, R., Pliner, H.A., Christiansen, L., Qiu, X., Steemers, F.J., et al. (2018). The cis-regulatory dynamics of embryonic development at single-cell resolution. Nature *555*, 538–542.

Davidson, J. (1944). On the relationship between temperature and rate of development of insects at constant temperatures. J. Anim. Ecol. 13, 26–38.

Davidson, E.H., and Erwin, D.H. (2006). Gene regulatory networks and the evolution of animal body plans. Science *311*, 796–800.

Ebert, M.S., and Sharp, P.A. (2012). Roles for microRNAs in conferring robustness to biological processes. Cell 149, 515–524.

Ebisuya, M., and Briscoe, J. (2018). What does time mean in development? Development 145, 1–6.

Felkai, S., Ewbank, J.J., Lemieux, J., Labbé, J.C., Brown, G.G., and Hekimi, S. (1999). CLK-1 controls respiration, behavior and aging in the nematode *Caenorhabditis elegans*. EMBO J. *18*, 1783–1792.

Ferrus, A. (1975). Parameters of mitotic recombination in *Minute* mutants of *Drosophila melanogaster*. Genetics 79, 589–599.

Foe, V.E. (1989). Mitotic domains reveal early commitment of cells in *Drosophila* embryos. Development *107*, 1–22.

Francesconi, M., and Lehner, B. (2014). The effects of genetic variation on gene expression dynamics during development. Nature 505, 208–211.

Gillespie, D.T. (1977). Exact stochastic simulation of coupled chemical-reactions. J. Phys. Chem. *81*, 2340–2361.

Gillooly, J.F., Charnov, E.L., West, G.B., Savage, V.M., and Brown, J.H. (2002). Effects of size and temperature on developmental time. Nature *417*, 70–73.

Giri, R., Papadopoulos, D.K., Posadas, D.M., Potluri, H.K., Tomancak, P., Mani, M., and Carthew, R.W. (2019). Stochastic noise in gene expression is optimized to drive developmental self-organization. bioRxiv. https://doi.org/10.1101/546911.

Golic, M.M., and Golic, K.G. (1996). A quantitative measure of the mitotic pairing of alleles in *Drosophila melanogaster* and the influence of structural heterozygosity. Genetics *143*, 385–400.

Graham, T.G., Tabei, S.M., Dinner, A.R., and Rebay, I. (2010). Modeling bistable cell-fate choices in the *Drosophila* eye: qualitative and quantitative perspectives. Development *137*, 2265–2278.

Graifer, D., Malygin, A., Zharkov, D.O., and Karpova, G. (2014). Eukaryotic ribosomal protein S3: A constituent of translational machinery and an extraribosomal player in various cellular processes. Biochimie *99*, 8–18.

Ikeya, T., Galic, M., Belawat, P., Nairz, K., and Hafen, E. (2002). Nutrient-dependent expression of insulin-like peptides from neuroendocrine cells in the CNS contributes to growth regulation in *Drosophila*. Curr. Biol. *12*, 1293–1300.

Jafar-Nejad, H., Acar, M., Nolo, R., Lacin, H., Pan, H., Parkhurst, S.M., and Bellen, H.J. (2003). Senseless acts as a binary switch during sensory organ precursor selection. Genes Dev. 17, 2966–2978.

Jafar-Nejad, H., Tien, A.C., Acar, M., and Bellen, H.J. (2006). Senseless and Daughterless confer neuronal identity to epithelial cells in the *Drosophila* wing margin. Development *133*, 1683–1692.

Julian, R.J. (2005). Production and growth related disorders and other metabolic diseases of poultry–a review. Vet. J. *169*, 350–369.

Kohwi, M., and Doe, C.Q. (2013). Temporal fate specification and neural progenitor competence during development. Nat. Rev. Neurosci. 14, 823–838.

Kozomara, A., and Griffiths-Jones, S. (2014). miRBase: annotating high confidence microRNAs using deep sequencing data. Nucleic Acids Res. 42, D68–D73.

Krafka, J. (1920). The effect of temperature upon facet number in the *Bar-Eyed* mutant of *Drosophila*: Part I. J. Gen. Physiol. 2, 409–432.

Kuntz, S.G., and Eisen, M.B. (2014). *Drosophila* embryogenesis scales uniformly across temperature in developmentally diverse species. PLoS Genet. *10*, e1004293.

Lanza, I.R., Zabielski, P., Klaus, K.A., Morse, D.M., Heppelmann, C.J., Bergen, H.R., 3rd, Dasari, S., Walrand, S., Short, K.R., Johnson, M.L., et al. (2012). Chronic caloric restriction preserves mitochondrial function in senescence without increasing mitochondrial biogenesis. Cell Metab. *16*, 777–788.

Lawrence, P. (1992). The Making of a Fly: The Genetics of Animal Design (Blackwell Scientific).

Layalle, S., Arquier, N., and Léopold, P. (2008). The TOR pathway couples nutrition and developmental timing in *Drosophila*. Dev. Cell *15*, 568–577.

Lee, C.H., Kiparaki, M., Blanco, J., Folgado, V., Ji, Z., Kumar, A., Rimesso, G., and Baker, N.E. (2018a). A regulatory response to ribosomal protein mutations controls translation, growth, and cell competition. Dev. Cell *46*, 456–469.

Lee, J.J., Sanchez-Martinez, A., Zarate, A.M., Benincá, C., Mayor, U., Clague, M.J., and Whitworth, A.J. (2018b). Basal mitophagy is widespread in *Drosophila* but minimally affected by loss of Pink1 or parkin. J. Cell Biol. 217. 1613–1622.

Lempiäinen, H., and Shore, D. (2009). Growth control and ribosome biogenesis. Curr. Opin. Cell Biol. 21, 855–863.

Levavasseur, F., Miyadera, H., Sirois, J., Tremblay, M.L., Kita, K., Shoubridge, E., and Hekimi, S. (2001). Ubiquinone is necessary for mouse embryonic development but is not essential for mitochondrial respiration. J. Biol. Chem. *276*, 46160–46164.

Lewis, R.A., Wakimoto, B.T., Denell, R.E., and Kaufman, T.C. (1980). Genetic analysis of the *Antennapedia* gene complex (*Ant-C*) and adjacent chromosomal regions of *Drosophila melanogaster*. II. Polytene chromosome segments 84A-84B1,2. Genetics 95, 383–397.

Li, X., and Carthew, R.W. (2005). A microRNA mediates EGF receptor signaling and promotes photoreceptor differentiation in the *Drosophila* eye. Cell *123*, 1267–1277

Li, Y., Wang, F., Lee, J.A., and Gao, F.B. (2006). MicroRNA-9a ensures the precise specification of sensory organ precursors in *Drosophila*. Genes Dev. *20*, 2793–2805.

Li, X., Cassidy, J.J., Reinke, C.A., Fischboeck, S., and Carthew, R.W. (2009). A microRNA imparts robustness against environmental fluctuation during development. Cell 137, 273-282.

Lohmann, I., McGinnis, N., Bodmer, M., and McGinnis, W. (2002). The Drosophila Hox gene deformed sculpts head morphology via direct regulation of the apoptosis activator reaper. Cell 110, 457-466.

López-Lluch, G., Hunt, N., Jones, B., Zhu, M., Jamieson, H., Hilmer, S., Cascajo, M.V., Allard, J., Ingram, D.K., Navas, P., and de Cabo, R. (2006). Calorie restriction induces mitochondrial biogenesis and bioenergetic efficiency. Proc. Natl. Acad. Sci. USA 103, 1768-1773.

Lu, C., Brauer, M.J., and Botstein, D. (2009). Slow growth induces heat-shock resistance in normal and respiratory-deficient yeast. Mol. Biol. Cell 20, 891-903.

Marygold, S.J., Roote, J., Reuter, G., Lambertsson, A., Ashburner, M., Millburn, G.H., Harrison, P.M., Yu, Z., Kenmochi, N., Kaufman, T.C., et al. (2007). The ribosomal protein genes and Minute loci of Drosophila melanogaster. Genome Biol. 8, R216.

Metcalfe, N.B., and Monaghan, P. (2001). Compensation for a bad start: grow now, pay later? Trends Ecol. Evol. 16, 254-260.

Milo, R., and Phillips, R. (2016). Cell Biology by the Numbers (Garland Science).

Morgan, T.H. (1915). The mechanism of Mendelian heredity (Holt).

Morgan, T.H. (1929). Variability in eyeless. Carnegie Inst. Wash. Publ. 399, 139-168

Moss, E.G. (2007). Heterochronic genes and the nature of developmental time. Curr. Biol. 17, R425-R434.

Nakai, D., Yuasa, S., Takahashi, M., Shimizu, T., Asaumi, S., Isono, K., Takao, T., Suzuki, Y., Kuroyanagi, H., Hirokawa, K., et al. (2001). Mouse homologue of coq7/clk-1, longevity gene in Caenorhabditis elegans, is essential for coenzyme Q synthesis, maintenance of mitochondrial integrity, and neurogenesis. Biochem. Biophys. Res. Commun. 289, 463-471.

Neumann, C.J., and Cohen, S.M. (1996). Sternopleural is a regulatory mutation of wingless with both dominant and recessive effects on larval development of Drosophila melanogaster. Genetics 142, 1147-1155.

Nolo, R., Abbott, L.A., and Bellen, H.J. (2000). Senseless, a Zn finger transcription factor, is necessary and sufficient for sensory organ development in Drosophila. Cell 102, 349-362.

Peláez, N., Gavalda-Miralles, A., Wang, B., Navarro, H.T., Gudjonson, H., Rebay, I., Dinner, A.R., Katsaggelos, A.K., Amaral, L.A., and Carthew, R.W. (2015). Dynamics and heterogeneity of a fate determinant during transition towards cell differentiation. eLife 4, e08924.

Pontzer, H., Brown, M.H., Raichlen, D.A., Dunsworth, H., Hare, B., Walker, K., Luke, A., Dugas, L.R., Durazo-Arvizu, R., Schoeller, D., et al. (2016). Metabolic acceleration and the evolution of human brain size and life history. Nature 533,

Poullet, N., Vielle, A., Gimond, C., Carvalho, S., Teotónio, H., and Braendle, C. (2016). Complex heterochrony underlies the evolution of Caenorhabditis elegans hermaphrodite sex allocation. Evolution 70, 2357-2369.

Pressman, S., Reinke, C.A., Wang, X., and Carthew, R.W. (2012). A systematic genetic screen to dissect the microRNA pathway in Drosophila. G3 (Bethesda) 2 437-448

Quan, X.J., and Hassan, B.A. (2005). From skin to nerve: flies, vertebrates and the first helix. Cell. Mol. Life Sci. 62, 2036-2049.

Rebay, I., and Rubin, G.M. (1995). Yan functions as a general inhibitor of differentiation and is negatively regulated by activation of the Ras1/MAPK pathway. Cell 81, 857-866.

Rulifson, E.J., Kim, S.K., and Nusse, R. (2002). Ablation of insulin-producing neurons in flies: growth and diabetic phenotypes. Science 296, 1118-1120.

Rutherford, S.L., and Lindquist, S. (1998). Hsp90 as a capacitor for morphological evolution, Nature 396, 336-342.

Saebøe-Larssen, S., Lyamouri, M., Merriam, J., Oksvold, M.P., and Lambertsson, A. (1998). Ribosomal protein insufficiency and the Minute syndrome in Drosophila: a dose-response relationship. Genetics 148, 1215–1224.

Sang, J.H., and Burnet, B. (1963). Environmental modification of the eyeless phenotype in Drosophila melanogaster. Genetics 48, 1683-1699.

Shingleton, A.W., Das. J., Vinicius, L., and Stern, D.L. (2005), The temporal requirements for insulin signaling during development in Drosophila. PLoS Biol. 3. e289.

Sulston, J.E., Schierenberg, E., White, J.G., and Thomson, J.N. (1983). The embryonic cell lineage of the nematode Caenorhabditis elegans. Dev. Biol. 100, 64-119.

Tang, H.Y., Smith-Caldas, M.S., Driscoll, M.V., Salhadar, S., and Shingleton, A.W. (2011). FOXO regulates organ-specific phenotypic plasticity in *Drosophila*. PLoS Genet. 7, e1002373.

Van Doren, M., Bailey, A.M., Esnayra, J., Ede, K., and Posakony, J.W. (1994). Negative regulation of proneural gene activity: Hairy is a direct transcriptional repressor of achaete. Genes Dev. 8, 2729-2742.

Venken, K.J., He, Y., Hoskins, R.A., and Bellen, H.J. (2006). P[acman]: a BAC transgenic platform for targeted insertion of large DNA fragments in D. melanogaster. Science 314, 1747-1751.

Villee, C. (1943). Phenogenetic studies of the homoeotic mutants of Drosophila melanogaster. 1. The effects of temperature on the expression of aristapedia. J. Exp. Zool. 93, 75-98.

Voas, M.G., and Rebay, I. (2004). Signal integration during development: insights from the Drosophila eye. Dev. Dyn. 229, 162-175.

Webb, A.E., and Brunet, A. (2014). FOXO transcription factors: key regulators of cellular quality control. Trends Biochem. Sci. 39, 159-169.

Webber, J.L., Zhang, J., Cote, L., Vivekanand, P., Ni, X., Zhou, J., Nègre, N., Carthew, R.W., White, K.P., and Rebay, I. (2013). The relationship between long-range chromatin occupancy and polymerization of the Drosophila ETS family transcriptional repressor Yan. Genetics 193, 633-649.

Whitehead, C.C., Fleming, R.H., Julian, R.J., and Sørensen, P. (2003). Skeletal problems associated with selection for increased production. In Poultry Genetics, Breeding and Biotechnology, W.M. Muir and S.E. Aggrey, eds. (CABI Publishing), pp. 29-52.

Wolff, T., and Ready, D. (1993). Pattern formation in the Drosophila retina. In The Development of Drosophila melanogaster, M. Bate and A. Martinez-Arias, eds. (Cold Spring Harbor Press), pp. 1277-1325.

Wong, A., Boutis, P., and Hekimi, S. (1995). Mutations in the clk-1 gene of Caenorhabditis elegans affect developmental and behavioral timing. Genetics 139, 1247-1259.

Zhang, H., Liu, J., Li, C.R., Momen, B., Kohanski, R.A., and Pick, L. (2009). Deletion of Drosophila insulin-like peptides causes growth defects and metabolic abnormalities. Proc. Natl. Acad. Sci. USA 106, 19617-19622.

Zuo, W., Moses, M.E., West, G.B., Hou, C., and Brown, J.H. (2012). A general model for effects of temperature on ectotherm ontogenetic growth and development. Proc. Biol. Sci. 279, 1840-1846.

STAR***METHODS**

KEY RESOURCES TABLE

REAGENT or RESOURCE	SOURCE	IDENTIFIER
Antibodies		
Mouse monoclonal anti-Prospero	Developmental Studies Hybridoma Bank	MR1A mAb; RRID: AB_528440
Rat monoclonal anti-Elav	Developmental Studies Hybridoma Bank	7E8A10 mAb; RRID: AB_528218
Goat anti-mouse Alexa488	Invitrogen	A-11001; RRID: AB_2534069
Goat anti-rat Alexa546	Invitrogen	A-11081; RRID: AB_2534125
Goat anti-mouse Alexa546	Invitrogen	A-11030; RRID: AB_2534089
Goat anti-rat Alexa633	Invitrogen	A-21094; RRID: AB_2535749
Mouse monoclonal anti-ATP5A (MAb15H4C4)	Abcam	ab14748; RRID: AB_301447
Chemicals, Peptides, and Recombinant Proteins		
Paraformaldehyde (powder)	Polysciences	00380-1
Triton X-100	Sigma Aldrich	T9284-500ML
VectaShield	Vector Labs	H-1000
4',6-diamidino-2-phenylindole (DAPI)	Life Technologies	D1306
Deposited Data		
Data of all model simulations	This paper	https://arch.library.northwestern.edu/concern/generic_works/n296wz31t
Fluorescence data for Yan-YFP and His2Av- mRFP in eye cells	This paper	https://arch.library.northwestern.edu/concern/generic_works/n296wz31t
Fluorescence data for sfGFP-Sens in wing cells	This paper	https://www.dropbox.com/ sh/1m9silkrs76rvpr/ AADunGcGUylP2rQ9WRo5bXVha?dl=0
Experimental Models: Organisms/Strains		
<i>D. melanogaster: mir-9a</i> ^{E39} Swap of the pre-miRNA sequence with <i>white</i> ⁺ . RNA null.	Li et al., 2006	N/A
D. melanogaster: mir-9a ^{J22} Swap of the pre-miRNA sequence with white ⁺ . RNA null.	Li et al., 2006	N/A
D. melanogaster: mir-7 ^{∆1} Deletion of pre-miRNA sequence. RNA null.	Li and Carthew, 2005	N/A
D. melanogaster: Df(2R)exu1 cn[1] bw[1] Deletion	Bloomington Drosophila Stock Center	BDSC: 1510
of pre-miR-7 sequence. RNA null		Flybase: FBab0002178
D. melanogaster: dcr-1 ^{K43X} Nonsense mutation at residue 43. Amorph.	Pressman et al., 2012	N/A
<i>D. melanogaster: dcr-1</i> ^{W94X} Nonsense mutation at residue 94. Amorph.	Pressman et al., 2012	N/A
D. melanogaster: dcr-1 ^{Q396X} Nonsense mutation at residue 396. Amorph.	Pressman et al., 2012	N/A
D. melanogaster: dcr-1 ^{Q1147X} Nonsense mutation at residue 1147. Amorph.	Pressman et al., 2012	N/A
D. melanogaster: ago1 ^{Q127X} Nonsense mutation at residue 127. Protein null.	Pressman et al., 2012	N/A
D. melanogaster: ago1 ^{W894X} Nonsense mutation at residue 894. Protein null.	Pressman et al., 2012	N/A
D. melanogaster: ago1 ^{T908M} Missense T-to-M mutation at residue 908.	Pressman et al., 2012	N/A
D. melanogaster: ago1 ^{E808K} Missense E-to-K mutation at residue 808.	Pressman et al., 2012	N/A
D. melanogaster: ago1 ^{R937C} Missense R-to-C mutation at residue 937.	Pressman et al., 2012	N/A
		(Continued on next page

(Continued on next page)

Continued		
REAGENT or RESOURCE	SOURCE	IDENTIFIER
D. melanogaster: w ¹¹¹⁸	Bloomington Drosophila Stock Center	BDSC: 3605
		Flybase: FBst0003605
D. melanogaster: hairy ¹ Insertion of gypsy TE	Bloomington Drosophila Stock Center	BDSC: 513
in the <i>hairy</i> promoter. Hypomorph.		Flybase: FBst0000513
D. melanogaster: hairy ⁴¹ Nonsense mutation	Bloomington Drosophila Stock Center	BDSC: 5337
at residue 114. Protein null.		Flybase: FBst0005337
D. melanogaster: sev14 also called sevd2 EMS	Bloomington Drosophila Stock Center	BDSC: 10546
induced. Protein null.		Flybase: FBal0015458
D. melanogaster: wg ^{Sp-1} Mutation in the	Bloomington Drosophila Stock Center	BDSC: 8379
3' regulatory CRM of wg. Gain of function (Neumann and Cohen, 1996)		Flybase: FBst0008379
D. melanogaster: RpS3 ^{Plac92}	Bloomington Drosophila Stock Center	BDSC: 5627
P element insertion mutant		Flybase: FBst0005627
D. melanogaster: RpS3 ²	Bloomington Drosophila Stock Center	BDSC: 1696
		Flybase: FBst0001696
D. melanogaster: RpS13 ¹	Bloomington Drosophila Stock Center	BDSC: 2246
P element insertion mutant		Flybase: FBst0002246
D. melanogaster: RpS15 ^{M(2)53}	Bloomington Drosophila Stock Center	BDSC: 346
Synonym M(2)53[1]		Flybase: FBst0000346
D. melanogaster: yan ^{ACT} Transgenic P element: Yan (Aop) CDS with all MAPK phosphorylation sites mutated; with 3'UTR lacking miR-7 binding sites, transcription under heterologous GMR promoter control.	Rebay and Rubin, 1995	N/A
D. melanogaster: yan ^{WT} Transgenic P element: Yan (Aop) CDS with with 3'UTR lacking miR-7 binding sites, transcription under heterologous GMR promoter control.	Rebay and Rubin, 1995	N/A
D. melanogaster: Yan-YFP [attP2] Pacman construct containing yan (aop) locus with C-terminal YFP fusion.	Webber et al., 2013	N/A
D. melanogaster: Yan ^{4miR-7} -YFP [attP2] Pacman construct containing yan (aop) locus with C-terminal YFP fusion and 4 miR-7 binding sites mutated.	This paper	N/A
D. melanogaster: sfGFP-sens [VK37] Pacman construct containing sens locus with N-terminal sfGFP fusion.	Venken et al., 2006	N/A
D. melanogaster: sfGFP-sens ^{m1m2} [VK37] Pacman construct containing sens locus with N-terminal sfGFP fusion and 2 miR-9a binding sites mutated.	Giri et al., 2019	N/A
D. melanogaster: w ey-FLP; FRT42D mir-7 ^{Δ1} / FRT42D GMR-Hid cl.	Li and Carthew, 2005	N/A
D. melanogaster: w ey-FLP; FRT42D ago1 ^{W894} / FRT42D GMR-Hid cl	Pressman et al., 2012	N/A
D. melanogaster: w ey-FLP; FRT42D w⁺	Bloomington Drosophila Stock Center	BDSC: 1928
		Flybase: FBst0001928
D. melanogaster: w ey-FLP; FRT42D	Bloomington Drosophila Stock Center	BDSC: 5251
GMR-Hid cl		Flybase: FBst0005251
D. melanogaster: w P{ey-FLP.N} ; ; ry	Bloomington Drosophila Stock Center	BDSC: 5576
D. Illelanogaster. W F (ey-1 LF.N), , Ty		

(Continued on next page)

Continued		
REAGENT or RESOURCE	SOURCE	IDENTIFIER
D. melanogaster: w; P{His2Av-mRFP1}	Bloomington Drosophila Stock Center	BDSC: 23650
Fusion of His2Av histone and RFP driven by the His2Av promoter.		Flybase: FBst0023650
D. melanogaster: w; P{ILP2-GAL4}	Bloomington Drosophila Stock Center	BDSC: 37516
		Flybase: FBst0037516
D. melanogaster: w; P{UAS-Rpr.C}	Bloomington Drosophila Stock Center	BDSC: 5824
		Flybase: FBst0005824
D. melanogaster: w P{UAS-Rpr.C}	Bloomington Drosophila Stock Center	BDSC: 5823
		Flybase: FBst0005823
Recombinant DNA		
P[acman] <i>Yan^{∆miR-7}-YFP</i>	This paper	N/A
P[acman] Yan-YFP	Webber et al., 2013	N/A
P[acman] sfGFP-sens	Venken et al., 2006	N/A
P[acman] sfGFP-sens ^{m1m2}	Giri et al., 2019	N/A
Software and Algorithms		
Code for the control theory modeling and analysis@	This paper	https://github.com/sebastianbernasek/
Older pipeline for segmentation and analysis of nuclear fluorescence in imaginal discs	Peláez et al., 2015	https://www.dropbox.com/s/ 62i91i17c9ja1c5/Pipeline_eye_eLife. zip?dl=0
FlyEye Silhouette Suite: Newest software for segmentation and analysis of nuclear fluorescence in imaginal discs	This paper	https://www.silhouette.amaral. northwestern.edu/

LEAD CONTACT AND MATERIALS AVAILABILITY

Further information and requests for resources and reagents should be directed to and will be fulfilled by the Lead Contact, Richard Carthew (r-carthew@northwestern.edu).

EXPERIMENTAL MODEL AND SUBJECT DETAILS

Drosophila Growth and Genetics

For all experiments, Drosophila melanogaster was raised using standard lab conditions and food. All experiments used female animals unless stated otherwise. Stocks were either obtained from the Bloomington Stock Center, from listed labs, or were derived in our laboratory (RWC). A list of all mutants and transgenics used in this study is in the Key Resources Table.

Experiments were performed using either homozygous mutant animals or trans-heterozygous mutants. Trans-heterozygous allele combinations used were:

```
mir-9a<sup>E39</sup>/mir-9a<sup>J22</sup>
hairy<sup>1</sup>/hairy<sup>41</sup>
wg^{Sp-1}/wg^+
mir-7<sup>∆1</sup>/Df(2R)exu1
dcr-1+/dcr-1Q1147X
dcr-1<sup>K43X</sup>/dcr-1<sup>Q1147X</sup>
dcr-1W94X/dcr-1Q1147X
dcr-1<sup>Q396X</sup>/dcr-1<sup>Q1147X</sup>
ago1<sup>+</sup>/ago1<sup>Q127X</sup>
ago1<sup>W894X</sup>/ago1<sup>Q127X</sup>
ago1<sup>T908M</sup>/ago1<sup>Q127X</sup>
ago1<sup>E808K</sup>/ago1<sup>Q127X</sup>
ago1<sup>R937C</sup>/ago1<sup>Q127X</sup>
```

To genetically ablate the insulin producing cells (IPCs) of the brain, yw animals were constructed bearing an ILP2-GAL4 gene on chromosome III and a UAS-Reaper (Rpr) gene on chromosome I or II. Rpr is a pro-apoptotic gene that is sufficient to kill cells in which it is expressed (Lohmann et al., 2002). ILP2-GAL4 fuses the insulin-like peptide 2 gene promoter to GAL4, and specifically drives its expression in brain IPCs (Rulifson et al., 2002). Examination of ILP2-GAL4 UAS-Rpr larval brains showed that they almost completely lacked IPCs (data not shown). Previous studies found that IPC-deficient adults are normally proportioned but of smaller size (Rulifson et al., 2002). It takes almost twice the length of time to complete juvenile development, and juveniles have a 40% elevation in blood glucose, consistent with insulin-like peptides (ILPs) being essential regulators of glucose metabolism in Drosophila (Broughton et al., 2005; Ikeya et al., 2002; Rulifson et al., 2002). We confirmed that this method of IPC ablation results in small but normally proportioned adults, and it takes almost twice the normal time to develop into adults (Figures 1B and 1C). We also examined whether IPC ablation reduced mitochondrial respiration. We did this by immunostaining larval wing imaginal disc peripodial cells for the alpha subunit of mitochondrial ATP synthase. The alpha subunit is a core of the ATP synthase complex that resides in the inner membrane and protrudes into the matrix. Wild-type peripodial cell mitochondria appear highly reticulated, whereas mitochondria from IPC-ablated tissue appear fragmented (Figure S1). Moreover, ATP synthase abundance is reduced in cells from IPC-ablated larvae. These observations are consistent with the effects of caloric restriction on mitochondria; the mitochondria membrane potential is reduced (López-Lluch et al., 2006), and abundance of proteins involved in oxidative phosphorylation, including Complex V subunits are reduced (Lanza et al., 2012). For all wild-type controls, we tested animals bearing either the ILP2-GAL4 or UAS-Rpr gene in their genomes.

The IPCs synthesize and release three ILPs to regulate glucose metabolism (Brogiolo et al., 2001; Broughton et al., 2005; Ikeya et al., 2002). To rule out the possibility that other hormones in IPCs are responsible for the metabolic, growth and developmental phenotypes of IPC-ablated animals, a number of labs performed complementary experiments. Rulifson et al. (2002) showed that growth rate, developmental rate, and final body size of IPC-ablated animals were highly similar to animals that had a mutation in the gene that encodes the Insulin Receptor. Moreover, they ablated the IPCs and then ectopically expressed ILP2 in other cells. This rescued the growth rate, developmental rate, and final size of animals. Zhang et al. simultaneously mutated five of the ILP genes (Zhang et al., 2009). This mutant had a reduced growth rate and final body size that was highly similar to animals that had their IPCs ablated. Moreover, mutant animals generated 30% less heat output as measured by whole-body calorimetry (Zhang et al., 2009). Thus, genetic manipulation of ILP genes phenocopies and rescues IPC ablation, arguing that loss of ILP expression is the reason why IPC ablation has effects on growth, metabolism and size.

To reduce the rate of general protein synthesis in cells, we made use of loss-of-function mutations in genes encoding various ribosomal proteins (RPs), which cause the "Minute" syndrome of dominant, haploinsufficient phenotypes, including prolonged development (Saebøe-Larssen et al., 1998). A total of 64 RP genes exhibit a Minute syndrome when mutated (Marygold et al., 2007). We selected a subset of these genes to reduce protein synthesis rate. Since one of these, RpS3, encodes an RP that also functions in DNA repair (Graifer et al., 2014), we tested it along with other RP genes in certain genetic experiments. The mutations used were: RpS3^{Plac92} (Saebøe-Larssen et al., 1998), RpS3² (Ferrus, 1975), RpS13¹ (Saebøe-Larssen et al., 1998), and RpS15^{M(2)53} (Golic and Golic, 1996). For wild-type controls, animals were w^{1118} .

To test for suppression of microRNA phenotypes by RP mutation we attempted to combine six RP mutants with ago1 and dcr-1 alleles. However, all were unilaterally lethal or sterile during the construction phase of the process, and we were unsuccessful. Minute mutants are dominant and sick, so this outcome was not surprising; indeed, difficulties were also encountered in constructing RP mutants with the individual repressor gene mutants.

Transgenesis

The recombineered Yan-YFP BAC transgene was previously described (Webber et al., 2013). We modified the gene by site-directed recombineering to mutate the four identified miR-7 binding sites within the yan (aop) gene (Li and Carthew, 2005). The binding sites and the mutations are listed below. The seed sequence is highlighted in bold. The sequence of the mutations, which are localized to the seeds, are shown in bold below each binding site sequence.

```
Site 1 chr2L: 2,158,120 - 2,158,124
5'-TCACCGCACTACATCCATCTTCCA-3'
        ATAGGAAA
Site 2 chr2L: 2,157,048 - 2,157,052
5'-ATAGAAAAACATTGGCTTCCA-3'
        GGAGGAAA
Site 3 chr2L: 2,156,854 - 2,156,858
5'-ACGATCTTACCACCACACTTCCA-3'
         CAAGGAAA
Site 4 chr2L: 2,156,564 - 2,156,568
5'-TCGCCACAATACCTGTTCTTCCA-3'
         TTAGGAAA
```

The mutated transgene ($Yan^{\Delta miR-7}$ -YFP) was shuttled into the P[acman] vector (Venken et al., 2006), and inserted into the same genomic landing site on chromosome 3 (attP2) as Yan-YFP. One copy of the His2Av-mRFP transgene was recombined with the $Yan^{\Delta miR-7}$ -YFP or Yan-YFP transgene in order to normalize YFP expression to a housekeeping protein, in this case histone H2A (Peláez et al., 2015). The His2Av-mRFP Yan-YFP ($Yan^{\Delta miR-7}$ -YFP) chromosome was homozygosed, and placed in a Yan^{ER443} / Yan^{E884} mutant background so that the endogenous Yan gene did not make any protein.

The recombineered *sfGFP-sens* BAC transgene was generated as described (Cassidy et al., 2013), and the transgene was landed in the genome at VK37 (22A3). The transgene was mutated by site-directed recombineering as described (Cassidy et al., 2013) to delete the two miR-9a binding sites within the *sens* gene (*sfGFP-sens*^{m1m2}). This transgene was also landed at VK37. The *sfGFP-sens* (*sfGFP-sens*^{m1m2}) chromosome was homozygosed, and placed in a *sens*^{E1} mutant background to ensure that endogenous *sens* made almost no protein.

METHOD DETAILS

R7 Cell Analysis in the Eye

Individuals were synchronized at the larval-pupal transition, and incubated for a further 48 hours at 23°C. Eyes were dissected from pupae in ice-cold Phosphate Buffered Saline (PBS), and were fixed for 40 min in 4% paraformaldehyde/PBS. They were permeabilized by incubation in PBS + 0.1% Triton X-100 (PBST) and co-incubated with mouse anti-Prospero (1:10 in PBST, MR1A mAb, Developmental Studies Hybridoma Bank) to stain R7 and bristle cells plus rat anti-Elav (1:10 in PBST, 7E8A10 mAb, Developmental Studies Hybridoma Bank) to stain all R cells. After 60 min, eyes were washed 3 times in PBST and incubated for 60 min in goat anti-mouse Alexa546 and goat anti-rat Alexa633 (1:100 in PBST, Invitrogen). Eyes were washed 3 times in PBST, cleared in Vectashield (Vector Labs), and mounted for microscopy. Samples were scanned and imaged in a Leica SP5 confocal microscopy system. *Drosophila* compound eyes have approximately 800 ommatidia. We scored all ommatidia for each imaged eye sample. The number of scored ommatidia per sample ranged between 481 and 837 (with a median of 594). Fewer than 800 ommatidia were scored per sample because in most cases, some eye tissue was lost during dissection and handling.

Relative Viability

Females bearing either a $dcr-1^{Q1147X}$ or $ago1^{Q127X}$ mutant chromosome over a balancer chromosome were crossed to males bearing mutant dcr-1 or ago1 chromosomes over a balancer chromosome. F1 progeny were raised and the numbers of animals that reached either pupal or adult stage were tallied. If the non-balancer chromosome is 100% viable when homozygous, then 33.33% of the F1 progeny would not carry a balancer chromosome. We calculated viability in this manner, relative to balancer viability. Replicate crosses were performed and analyzed. Between 457 and 776 F1 animals (median = 647) were counted in the replicate ago1 crosses. Between 234 and 380 F1 animals (median = 285) were counted in the replicate dcr-1 crosses.

Eye Mispatterning

Genetic mosaic animals bearing *mir*-7^{Δ1} homozygous mutant eyes were generated using the FLP-FRT system. The animals' genotype was: w ey-FLP; FRT42D mir-7^{Δ1} / FRT42D GMR-Hid cI. Matching wild-type control animals' genotype was: w ey-FLP; FRT42D $P[w^+]$ / FRT42D GMR-Hid cI. Individuals also contained either ILP2-GAL4 alone (control) or ILP2-GAL4 UAS-Rpr (IPC ablated) transgenes. All individuals were raised at 29°C. Eye roughening was scored as previously described (Li et al., 2009). Sample population sizes were between 264 and 467 individuals. For RpS3 interactions with mir-7, trans-heterozygous mir-7 mutants and matched wild-type controls (Df(2R)exu1/+) were raised at 29°C to adulthood. The $RpS3^2$ allele was combined with mir-7 alleles. Eye roughening was scored as previously described (Li et al., 2009). Genetic mosaic animals bearing $ago1^{W894}$ homozygous mutant eyes were generated using the FLP-FRT system. The animals' genotype was: w ey-FLP; FRT42D GMR-Hid cI. Matching wild-type control animals' genotype was: w ey-FLP; FRT42D GMR-Hid cI. Individuals also contained either ILP2-GAL4 alone (control) or ILP2-GAL4 UAS-Rpr (IPC ablated) transgenes. For experiments with Yan transgenics, animals bearing one copy of either the Yan^{ACT} or Yan^{WT} (Rebay and Rubin, 1995) transgene also contained either ILP2-GAL4 alone (control) or ILP2-GAL4 UAS-UAS

Bristle Scoring

Animals of the correct genotype were allowed to age for 3 days after eclosion. The number of scutellar bristles was counted for each individual. Since these large bristles are positioned with high regularity and number on the scutellum, there was no ambiguity in counting the scutellar bristle number. For wg experiments, the number of sternopleural bristles was counted for each individual. Again, the position and number of these bristles is highly regular.

Quantification of sfGFP-Sens Expression in the Wing Disc

Wing discs from white-prepupal females were dissected out in ice-cold PBS. Discs were fixed in 4% paraformaldehyde in PBS for 20 minutes at 25°C and washed with PBS containing 0.3% Tween-20. Then they were stained with 0.5 µg/ml 4′,6-diamidino-2-phenylindole (DAPI) and mounted in Vectashield (Vector Labs). Discs were mounted apical side up and imaged with identical settings

using a Leica TCS SP5 confocal microscope. All images were acquired at 100x magnification at 2048 × 2048 resolution with a 75 nm x-y pixel size and 0.42 μm z separation. Scans were collected bidirectionally at 400 MHz and 6x line averaged. Wing discs of different genotypes were mounted on the same microscope slide and imaged in the same session for consistency in data quality.

For each wing disc, five optical slices containing Sens-positive cells along the anterior wing margin were chosen for imaging and analysis. See Data S1 for examples of typical image data. A previously documented custom MATLAB script was used to segment nuclei in each slice of the DAPI channel (Peláez et al., 2015). High intensity nucleolar spots were smoothed out to merge with the nuclear area to prevent spurious segmentation. Next, cell nuclei were identified by thresholding based on DAPI channel intensity. Segmentation parameters were optimized to obtain nuclei with at least 100 pixels and no more than 4000 pixels.

The majority of imaged cells did not reside within the proneural region, and therefore they displayed background levels of fluorescence scattered around some mean level. We calculated the "mean background" in the green channel of each disc individually. We did this by fitting a Gaussian distribution to the population and finding the mean of that fit. In order to separate sfGFP-Sens-positive cells, we chose a cut-off percentile based on the normal distribution, below which cells were deemed sfGFP-Sens-negative. We set this cut-off at the 84th percentile for all analysis since empirically it provided the most accurate identification of proneural cells (Giri et al., 2019). To normalize measurements across tissues and experiments, this value was subtracted from the total measured fluorescence for all cells in that disc. Only cells with values above the threshold for sfGFP fluorescence were assumed Sens positive (usually 30% of total cells) and carried forward for further analysis.

We analyzed > 10 replicate wing discs for each treatment. In total, we measured wild-type sfGFP-Sens expression in 50,788 cells from wild-type RpS13 discs and 18,945 cells from discs heterozygous mutant for RpS131. We measured mutant sfGFP-Sens^{m1m2} expression in 79,835 cells from wild-type RpS13 discs and 12,954 cells from discs heterozygous mutant for RpS13⁷. The probability density plots were bootstrapped 1000 times by sampling with replacement, and the 95% CI was calculated by computing the 2.5/97.5th percentile y-value of probability density for each x-value.

Quantification of Yan-YFP Expression Dynamics in the Eye

White-prepupal eye discs were dissected, fixed, and imaged by confocal microscopy for YFP and RFP fluorescence, as previously described (Peláez et al., 2015). Briefly, samples fixed in 4% paraformaldehyde/PBS were kept in the dark at -20°C and imaged no later than 18-24 hr after fixation. In all cases, 1024 x 1024 16-bit images were captured using a Leica SP5 confocal microscope equipped with 40X oil objective. During imaging, discs were oriented with the equator parallel to the x axis of the image. Optical slices were set at 0.8μm slices (45-60 optical slices) with an additional digital zoom of 1.2-1.4 to completely image eye discs from basal to apical surfaces. Images recorded a region of at least 6 rows of ommatidia on each side or the dorsal-ventral eye disc equator. All discs for a given condition were fixed, mounted, and imaged in parallel to reduce measurement error. Sample preparation, imaging, and analysis were not performed under blind conditions. See Data S1 for examples of typical image data.

Image data was processed for automatic segmentation and quantitation of RFP and YFP nuclear fluorescence as described (Peláez et al., 2015). Briefly, cell segmentation was performed using a H2Av-mRFP marker as a reference channel for identification of cell nuclei boundaries. Each layer of the reference channel was segmented independently. A single contour containing each unique cell was manually selected and assigned a cell type using a custom graphic user interface. For each annotated cell contour, expression measurements were obtained by normalizing the mean pixel fluorescence of the YFP channel by the mean fluorescence of the His-RFP channel. This normalization serves to mitigate variability due to potentially uneven sample illumination, segment area, and differences in protein expression capacity between cells. We assigned cell-type identities to segmented nuclei by using nuclear position and morphology, two key features that enable one to unambiguously identify eye cell types without the need for cell-specific markers (Wolff and Ready, 1993). This task was accomplished using FlyEye Silhouette; an open-source package for macOS that integrates our image segmentation algorithm with a GUI for cell type annotation. Subsequent analysis and visualization procedures were implemented in Python.

Cell positions along the anterior-posterior axis were mapped to developmental time as described previously (Peláez et al., 2015). This depends on two assumptions that have been extensively validated in the literature. One, the furrow proceeds at a constant velocity of one column of R8 neurons per two hours, and two, minimal cell migration occurs. For each disc, Delaunay triangulations were used to estimate the median distance between adjacent columns of R8 neurons. Dividing the furrow velocity by the median distance yields a single conversion factor from position along the anterior-posterior axis to developmental time. This factor was applied to all cell measurements within the corresponding disc. This method does not measure single cell dynamics, but rather aggregate dynamics across the developmental time course of cells in the eye.

Moving averages were computed by evaluating the median value among a collection of point estimates for the mean generated within a sliding time window. Each point estimate was generated via a hierarchical bootstrapping technique in which we resampled the set of eye discs, then resampled the aggregate pool of cell measurements between them. This novel method enhances our existing approach (Peláez et al., 2015) by capturing variation due to the discretized nature of eye disc sample collection. A window size of 500 seguential progenitor cells was used in all cases, but our conclusions are not sensitive to our choice of window size. Yan level measurements were pooled across multiple replicate eye discs. An automated approach was used to align these replicate samples in time. First, a disc was randomly chosen to serve as the reference population for the alignment of all subsequent replicates. Cells from each replicate disc were then aligned with the reference population by shifting them in time. The magnitude of this shift was determined by maximizing the cross-correlation of moving-average Yan-YFP expression Y(t) with the corresponding reference time series X(t). Rather than raw measurements, moving averages within a window of ten cells were used to improve robustness against noise. This operation amounts to:

$$\operatorname*{argmax}_{\mathit{dt}} E \left[\frac{(Y(t+\mathit{dt}) - \mu_{Y})(X(t+\mathit{dt}) - \mu_{X})}{\sigma_{Y} \sigma_{X}} \right]$$

where, μ and σ are the mean and standard deviation of each time series, and dt is the magnitude of the time shift.

Different experimental treatments (e.g., wild-type and miR-7 null) were aligned by first aligning the discs within each treatment, then aggregating all cells within each treatment and repeating the procedure with the first treatment serving as the reference. We analyzed four to seven replicate eye discs for each treatment in two separate experiments. In total, we measured wild-type Yan-YFP levels in 4,518 cells in normally metabolizing samples and 4,379 cells in slowly metabolizing samples. We measured mutant Yan^{ΔmiR-7}-YFP levels in 5,382 cells in normally metabolizing samples and 6,716 cells in slowly metabolizing samples.

ATP Synthase Immunofluorescence

Wandering third instar larvae were dissected and wing discs were fixed in 4% paraformaldehyde/PBS. Wing discs were permeabilized by incubation in PBST and co-incubated with 1:500 mouse anti-ATP5A (Abcam) to stain the alpha subunit of Complex V. The antibody has been demonstrated to react with Drosophila ATP synthase (Lee et al., 2018b). After 60 min, eyes were washed 3 times in PBST and incubated for 60 min in goat anti-mouse Alexa546 (1:100 in PBST, Invitrogen). Eyes were washed 3 times in PBST, counterstained with DAPI to visualize nuclei, and cleared in Vectashield (Vector Labs). The peripodial membrane of disc samples was imaged with a Leica SP5 confocal microscopy system.

Mathematical Modeling

Our modeling framework directly describes the emergent expression dynamics of a single gene within a cascade of developmental gene expression. It leverages two key concepts from control theory. The first is the notion of Lyapunov stability; that is, systems tend to remain near stable equilibria. The second is the Hartman-Grobman theorem, which posits that systems deviate approximately linearly about these fixed points (Arrowsmith and Place, 1992). We therefore developed a model that describes the time evolution of linear deviations about the basal protein level that exists before gene expression is induced and after it subsides.

Specifically, a linear time invariant system describes the time evolution of deviations (Δ) in activated DNA (ΔP), mRNA (ΔP), and protein (ΔP) state variables in response to a change in stimulus (ΔI) that induces gene activation. These discrete state variables depict the extent to which gene expression has deviated from its basal level at any point in time. Transitions between each of the variables' states are governed by the stochastic processes listed below.

Reaction	State Transition	Propensity	Parameter Value [min ⁻¹]
gene activation	$\Delta D \rightarrow \Delta D + 1$	k ₁ Δl	1
transcription	$\Delta R \rightarrow \Delta R + 1$	k ₂ ΔD	1
translation	$\Delta P \rightarrow \Delta P + 1$	k ₃ ΔR	1
gene deactivation	$\Delta D \rightarrow \Delta D - 1$	$\gamma_1 \Delta D$	1
transcript decay	$\Delta R \rightarrow \Delta R - 1$	$\gamma_2 \Delta R$	1×10^{-2}
protein decay	$\Delta P \rightarrow \Delta P - 1$	γ ₃ ΔΡ	1×10^{-3}

Borrowing a third concept from control theory, we assume all repressors exert proportional control on protein levels. In other words, we abstract all regulatory processes using linear feedback terms:

Reaction	State Transition	Propensity	Parameter Value [min ⁻¹]
transcriptional feedback	$\Delta D \rightarrow \Delta D - 1$	η ₁ ΔΡ	5.0×10^{-4}
post-transcriptional feedback	$\Delta R \rightarrow \Delta R - 1$	$\eta_2 \Delta P$	1.0×10^{-4}
post-translational feedback	$\Delta P \rightarrow \Delta P - 1$	η ₃ ΔΡ	5.0×10^{-4}

In the continuum limit, this model yields a deterministic system of differential equations:

$$\frac{d\Delta D}{dt} = k_1 \Delta I - \gamma_1 \Delta D - \sum_{i=1}^{N} \eta_1 \Delta P$$

$$\frac{d\Delta R}{dt} = k_2 \Delta D - \gamma_2 \Delta R - \sum_{i=1}^{N} \eta_2 \Delta P$$

$$\frac{d\Delta P}{dt} = k_3 \Delta R - \gamma_3 \Delta P - \sum_{i=1}^{N} \eta_3 \Delta P$$

Where k_i are activation, transcription, or translation rate constants, γ_i are degradation constants, η_i are feedback strengths, and each species may be subject to N independent repressors. In control parlance, three sequential first-order transfer functions with interspersed feedback relate input disturbances to deviations in output protein level (Figure S3A).

We contend that the Hartman-Grobman theorem holds for the processes under study, but we also recognize that transcriptional and regulatory kinetics are often described using nonlinear kinetics. Therefore, we also considered two nonlinear modeling frameworks, both of which recapitulated the same results (Figures S4F, S4G, S6F, and S6G).

Dependence of Model Parameters on Metabolic Conditions

IPC ablation reduces cellular glucose consumption. Presumably this would affect either the production and consumption of ATP, or the production and consumption of substrates for RNA and protein synthesis (or both). The precise effects are unknown, so we independently modeled each scenario. Since ATP concentration remains fairly constant when respiration is limited (Brown, 1992), ATP flux (and ATP synthesis) is assumed to decrease. Because transcription, translation, and protein degradation all require ATP turnover, we halved their rate parameters under conditions of reduced glucose consumption. Under conditions of reduced substrate availability for RNA/protein synthesis, we assumed that only transcription and translation rates are affected by limiting fluxes of nucleotides and amino acids. We assumed only the translation rate is affected under conditions of reduced RP gene expression. These assumptions are incorporated as changes to the model's rate parameters as listed below.

Parameter	Normal Metabolism	Reduced ATP Consumption	Reduced RNA/Protein Substrates	Reduced Protein Synthesis Rate
transcription rate constant	k ₂	$\frac{1}{2}$ k ₂	$\frac{1}{2}$ k ₂	k ₂
translation rate constant	k ₃	$\frac{1}{2}$ k ₃	$\frac{1}{2}$ k ₃	$\frac{1}{2}$ k ₃
protein decay rate constant	γ3	<u>1</u> γ3	γ3	γз

In all cases, feedback strengths were reduced in order to account for the intermediate processes abstracted by each feedback element. Feedback strength parameters (η_i) were reduced four-fold under conditions of reduced energy metabolism and reduced RNA/protein substrate availability. This scaling assumes that both transcription and translation occur within the arbitrarily complex regulatory motifs represented by each repressor. This is a reasonable assumption for repressor proteins such as transcription factors and kinases. For RNA repressors such as microRNAs, feedback strength parameters could instead be reduced only two-fold to account for their reduced transcription rates. However, microRNAs must be transcribed, processed, and act with effector proteins in order to repress their targets. From a control perspective, these reductions in feedback strength correspond to fourfold reduction of the transcriptional feedback gain (K_{C1}) and twofold reduction in the post-transcriptional and post-translational feedback gains (K_{C2} and K_{C3}). Feedback strength parameters (η_i) were only reduced two-fold under reduced protein synthesis conditions. This implies that the transcriptional and post-transcriptional feedback gains (K_{CI} and K_{C2}) decrease twofold while the post-translational feedback gain (K_{C3}) remains constant. Each of these dependencies are summarized below.

Parameter	Normal Metabolism	Reduced ATP Consumption	Reduced RNA/Protein Substrates	Reduced Protein Synthesis Rate
transcriptional feedback strength	η_1	$\frac{1}{4}\eta_1$	$\frac{1}{4}\eta_{1}$	$\frac{1}{2}\eta_1$
post-transcriptional feedback strength	η_2	$\frac{1}{4}\eta_{2}$	$\frac{1}{4}\eta_2$	$\frac{1}{2}\eta_{2}$
post-translational feedback strength	η_3	$\frac{1}{4}\eta_{3}$	$\frac{1}{4}\eta_3$	$\frac{1}{2}\eta_3$

Model Simulations

Default parameter values were based on approximate transcript and protein synthesis and turnover rates for animal cells reported in the literature (Milo and Phillips, 2016), while gene activation and decay rates were arbitrarily set to a significantly faster timescale. Default feedback strengths for repressors acting at the gene, transcript, or protein levels were chosen such that ~25%–50% of simulations failed to reach the threshold under normal conditions when one of two identical repressors was lost. Population-wide expression dynamics were estimated by simulating 5000 output trajectories in response to a three-hour transient step input to the gene activation rate. Simulations were performed using a custom implementation of the stochastic simulation algorithm (Gillespie, 1977). The algorithm constrains solutions to the set of discrete positive values, consistent with linearization about a basal level of zero gene activity. This simplifying assumption is based on the near-zero basal activities expected in the experimental systems, but is not required to support the conclusions of the model (Figures S4D and S6D).

Evaluation of Error Frequencies and Changes in Expression Dynamics

Gene expression trajectories were simulated both with (full repression) and without (partial repression) a second repressor. The time point at which the full-repression simulations mean level reached 30% of its maximum value was taken to be the commitment time. At this time, a threshold for developmental success was set at the 99th percentile of protein levels subject to full-repression. Error frequencies were obtained by evaluating the fraction of simulated protein levels that exceeded this threshold. Per this definition, the minimum possible error frequency is one percent. For simplicity we subtracted this percentage point from all reported error frequencies.

Protein expression dynamics were compared by evaluating the fraction of partially-repressed simulation trajectories in excess of the 99th percentile of fully-repressed trajectories at each point in time t. We refer to this overexpression value as E(t). These values were then averaged across the time course, beginning with the reception of the input signal and ending at the previously defined commitment time, τ .

Percent overexpression
$$\equiv \frac{100}{\tau} \int_0^{\tau} E(t) dt$$

Percent overexpression reflects the extent to which the expression dynamics differ between the two sets of simulated trajectories (Figures S5A–S5C).

Parameter Variation and Sensitivity to Model Assumptions

We conducted parameter sweeps to confirm the robustness of each computational result. In each sweep, all model parameters were varied across a ten-fold range ($\pm \sim$ three-fold). We quasi-randomly generated 2500 such parameter sets, then independently ran six sets of five thousand simulations for each: 1) full feedback with normal metabolism and translation, 2) partial feedback with normal metabolism and translation, 3) full feedback with reduced energy metabolism, 4) partial feedback with reduced energy metabolism, 5) full feedback with reduced protein synthesis. Full-repression systems were assigned two copies of each feedback element present in the corresponding partial-repression system. Error frequencies were evaluated as described above.

Each sweep sampled a nine-dimensional space. Projecting the results of all simulations onto each of the 36 orthogonal 2-D planes revealed that error frequency is greater than 1% for almost all combinations of parameter values (Figure S3B). While it helps illustrate our parameter sweep methodology, the 2-D visualization does not offer sufficient insight into the global trend to justify its complexity. We instead opted for a condensed 1-D projection, which clearly indicates that partial loss of repression induces an increase in error frequency across a broad parameter range (Figure S4A). We also varied the level of the success threshold, and confirmed that loss of a repressor increases developmental error irrespective of where the success threshold is set (Figure S3C). Repressor loss also increases protein levels throughout the time course for the vast majority of parameter sets (Figure S5C).

The difference in error frequency between simulations with normal metabolism and reduced metabolism are shown in Figures S4A and S4B for all parameter sets, while the corresponding difference between simulations with normal protein synthesis and reduced protein synthesis are shown in Figure S6A. There is a general trend of decreased error frequency with partial repression under reduced energy metabolism and reduced protein synthesis conditions, irrespective of where the threshold is set (Figures S4C and S6C). The difference in protein overexpression between simulations with normal versus reduced metabolism are shown for all parameter sets in Figure S5D, while the corresponding difference between simulations with normal and reduced protein synthesis are shown in Figure S6B. Most parameter sets show less overexpression with partial repression when either metabolism or protein synthesis are reduced.

Our conclusion also persists when a nonzero basal stimulus is introduced. We conducted an additional parameter sweep in which the stimulus consists of a transient step change between input values of $\Delta I = 0.1$ and $\Delta I = 1.0$. Simulations were carried out on an absolute basis, and were allowed sufficient time to reach a non-zero steady state before and after the stimulus was applied. The resultant protein level trajectories for each of the six sets of simulations were converted to deviation form by subtracting the

respective population-wide mean final value. Error frequencies were then evaluated as previously described. Despite the inclusion of a nonzero basal stimulus, error frequencies remained broadly suppressed under conditions of both reduced energy metabolism and reduced protein synthesis (Figures S4D and S6D).

The preceding simulations assume the stimulus (input) is a unit step that persists for three hours regardless of metabolic conditions. Alternatively, metabolic conditions might affect stimulus duration, particularly if the upstream processes responsible for the input are also governed by metabolically delayed processes. We find that the general prediction made by our model – that reduced energy metabolism and reduced protein synthesis limit sensitivity to loss of regulation - persists in roughly half of cases if we apply four-fold and two-fold extensions of input duration under reduced energy metabolism and reduced protein synthesis conditions, respectively (Figures S4E and S6E). Notably, in many cases scaling the input duration with metabolic condition yields the opposite effect. However, these instances correspond to simulations in which the extended stimulus yields output protein levels greater than those observed under normal metabolic conditions, suggesting that a four-fold increase in stimulus duration may be excessive.

Alternate Models

The number of active sites firing transcription within a cell is limited by gene copy number, but the activated-DNA state in our simple linear model is unbounded. To test whether error frequency suppression persists when an upper bound on gene activity is introduced, we considered a simple two-state transcription model whose deterministic representation is given by:

$$\frac{dG_{on}}{dt} = k_{G}G_{off}I - \gamma_{G}G_{on} - \sum_{r}^{N_{g}}\eta_{G}G_{on}P$$

$$\frac{dG_{off}}{dt} = -\frac{dG_{on}}{dt}$$

$$\frac{dR}{dt} = k_{R}G_{on} - \gamma_{R}R - \sum_{r}^{N_{r}}\eta_{R}P$$

$$\frac{dP}{dt} = k_{P}R - \gamma_{P}P - \sum_{r}^{N_{p}}\eta_{P}P$$

where G_{on} and G_{off} are the on- and off- states of a gene; I, R and P are the input, transcript, and protein levels; k_i , γ_i , and η_i are the synthesis, decay, and feedback rate constants for species i; and N_a , N_r , and N_p are the number of transcriptional, post-transcriptional, and post-translational repressors, respectively. Rate parameter dependencies upon metabolic and protein synthesis conditions were analogous to those used in the linear model, and are tabulated below.

Parameter	Normal Metabolism	Reduced Metabolism	Reduced Protein Synthesis
transcription rate constant	k _R	$\frac{1}{2}$ k _R	k _R
translation rate constant	k _P	1/2 k _P	$\frac{1}{2} k_{P}$
protein decay rate constant	Ϋ́P	<u>1</u> γ _P	ΥР
transcriptional feedback strength	η_{G}	<u>1</u> η _G	<u>1</u> η _G
post-transcriptional feedback strength	η_{R}	1/4η _R	<u>1</u> η _R
post-translational feedback strength	η_{P}	1/ ₄ η _P	<u>1</u> η _Ρ

We performed a parameter sweep of this model in which all simulations were initialized as diploid ($G_{off} = 2$). Despite the limitation placed on gene activity, error frequency remains elevated under normal growth conditions and broadly suppressed when metabolism or protein synthesis are reduced (Figures S4F and S6F).

Gene expression models also frequently utilize cooperative kinetics in order to capture the nonlinearities and thresholds encountered in transcriptional regulation. We reformulated our gene expression model in terms of Hill kinetics:

$$\frac{dR}{dt} = \frac{k_R}{1 + \left(\frac{1}{2I}\right)^H} \prod_{r}^{N_g} \left[\frac{1}{1 + \left(\frac{P}{K_r}\right)^{H_r}} \right] - \gamma_R R - \sum_{r}^{N_r} \eta_R P$$

$$\frac{dR}{dt} = k_P R - \gamma_P P - \sum_{r}^{N_p} \eta_P P$$

where I, R, and P are the input, transcript, and protein levels; k_i , γ_i , and η_i are the synthesis, decay, and linear feedback rate constants for species i; N_r , and N_p are the number of post-transcriptional, and post-translational linear repressors; H is a transcriptional Hill coefficient; and K_r and K_r are the half-maximal occupancy level and Hill coefficient of each of the N_g transcriptional repressors. The stimulus level corresponding to half-maximal transcription rate was fixed at 0.5 because we only consider a binary input signal. Rate parameters were again scaled with metabolic and protein synthesis conditions in a manner analogous to the linear model.

Parameter	Normal Metabolism	Reduced Metabolism	Reduced Protein Synthesis
transcription rate constant	k _R	$\frac{1}{2}$ k_R	k _R
translation rate constant	k _P	$\frac{1}{2}$ k_P	$\frac{1}{2}$ k _P
protein decay rate constant	γр	<u>1</u> γ _P	ΥР
post-transcriptional feedback strength	η_{R}	$\frac{1}{4}\eta_R$	<u>1</u> η _R
post-translational feedback strength	η _P	$\frac{1}{4}\eta_P$	$\frac{1}{2}\eta_{P}$

The half-maximal occupancy level and Hill coefficients of transcriptional repressors were assumed to be independent of growth rate. Another parameter sweep revealed that despite the incorporation of cooperative binding kinetics, error frequency remains elevated under normal metabolic conditions and is broadly suppressed when metabolism or protein synthesis are reduced (Figures S4G and S6G).

QUANTIFICATION AND STATISTICAL ANALYSIS

Population proportions were compared using a Chi-square test with Yates' correction and a Fisher's exact test. Both tests gave similar results. All tests involving multiple experimental groups were Bonferroni corrected. Analysis of sev experiments scoring R7 cells applied a one-way ANOVA with Bonferroni correction. Relative viabilities were compared using a Mann-Whitney-Wilcoxon test with Bonferroni correction. These tests were performed using Prism 7 (GraphPad) software. P values shown in figures are presented from tests with the most conservative value shown if more than one test was performed on data. * p < 0.05; ** p < 0.01; *** p < 0.001; *** p < 0.0001

Confidence intervals for the moving average of Yan-YFP expression were inferred from the 2.5th and 97.5th percentile of 1000 point estimates of the mean within each moving-average window. Point estimates were generated by bootstrap resampling with replacement of the expression levels within each window.

Analysis of sfGFP-Sens fluorescence was performed using two independent approaches. 1) For each genotype, 1000 point-estimates were made of the median fluorescence level in cells. Point estimates were generated by bootstrap resampling with replacement of the cell samples within each genotype. Point estimates from wild-type sfGFP-Sens were then randomly paired with point estimates from miR-9a-resistant sfGFP-Sens to derive a set of 1000 point-estimates of the fold-change in median sfGFP-Sens expression. Confidence intervals for the average fold-change in sfGFP-Sens expression were inferred from the 0.5th and 99.5th percentile of these point estimates. 2) The distributions of fluorescence from wild-type sGFP-sens and mutant sGFP-sens m1m2 cell populations were compared using a Mann-Whitney-Wilcoxon test implemented in R. By calculating the difference between all randomly paired cell samples from wild-type versus mutant, the location shift μ is estimated as the median of the difference between a sample from sfGFP-Sens and a sample from sfGFP-Sens m1m2 . Confidence intervals for the shift were inferred from the 2.5th and 97.5th percentile of the set of differences.

There was no exclusion of any data or subjects.

DATA AND CODE AVAILABILITY

Data Availability

The phenotype datasets generated and/or analyzed during the current study are available from the corresponding authors on request.

The dataset of all model simulations:

https://arch.library.northwestern.edu/concern/generic_works/n296wz31t

The Yan-YFP dataset: https://arch.library.northwestern.edu/concern/generic_works/n296wz31t

The sfGFP-Sens dataset:

https://www.dropbox.com/sh/1m9silkrs76rvpr/AADunGcGUylP2rQ9WRo5bXVha?dl=0

Code Availability

All code is publicly available at:

Modeling and analysis: https://github.com/sebastianbernasek/GRaM

Pipeline for Eye Silhouette imaging analysis: https://www.silhouette.amaral.northwestern.edu/

Older pipeline for imaging analysis: https://www.dropbox.com/s/62i91i17c9ja1c5/Pipeline_eye_eLife.zip?dl=0

Supplemental Figures

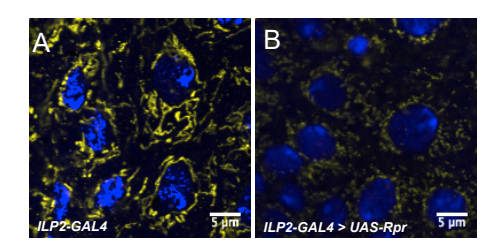


Figure S1. ATP Synthase Abundance Is Reduced in Cells of IPC-Ablated Larvae, Related to Figure 1

Shown are peripodial cells of wing imaginal discs from third instar larvae stained with an antibody recognizing the alpha subunit of mitochondrial ATP synthase (yellow). Cells have been counterstained with DAPI to highlight their nuclei (blue). ATP synthase localization and abundance are different between wild-type (A) and IPC-ablated (B) samples. Wild-type mitochondria appear highly reticulated, whereas mitochondria from IPC-ablated tissue appear fragmented. Moreover, ATP synthase abundance is reduced in the IPC-ablated tissue.

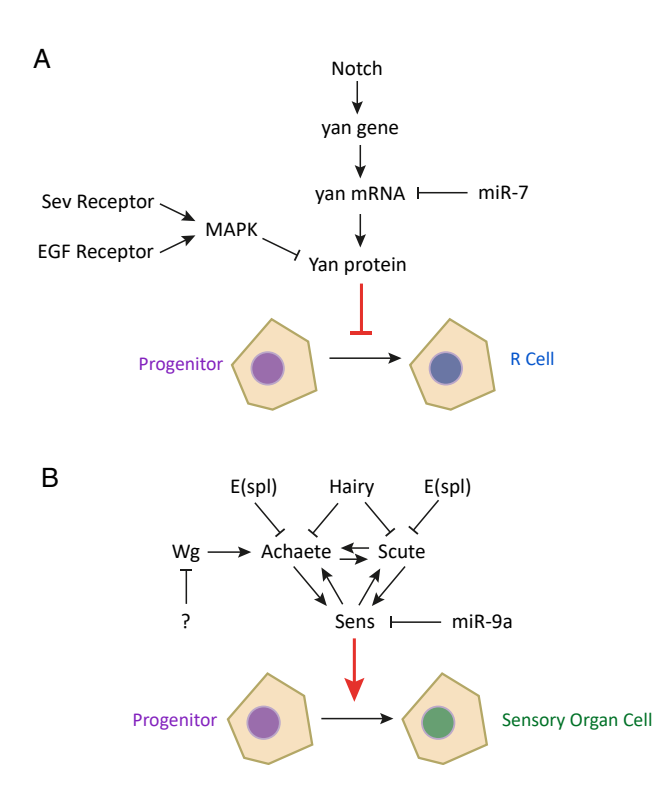


Figure S2. Schematics of Fate Determination of R and Sensory Organ Cells, Related to Figures 1 and 2

(A) Relevant transcription factors, microRNAs, and signaling factors involved in regulating R cell fate determination in the *Drosophila* eye. (B) Relevant transcription factors, microRNAs, and signaling factors involved in regulating determination of Sensory Organ Cells, which ultimately form many of the sensory bristles in the *Drosophila* adult.

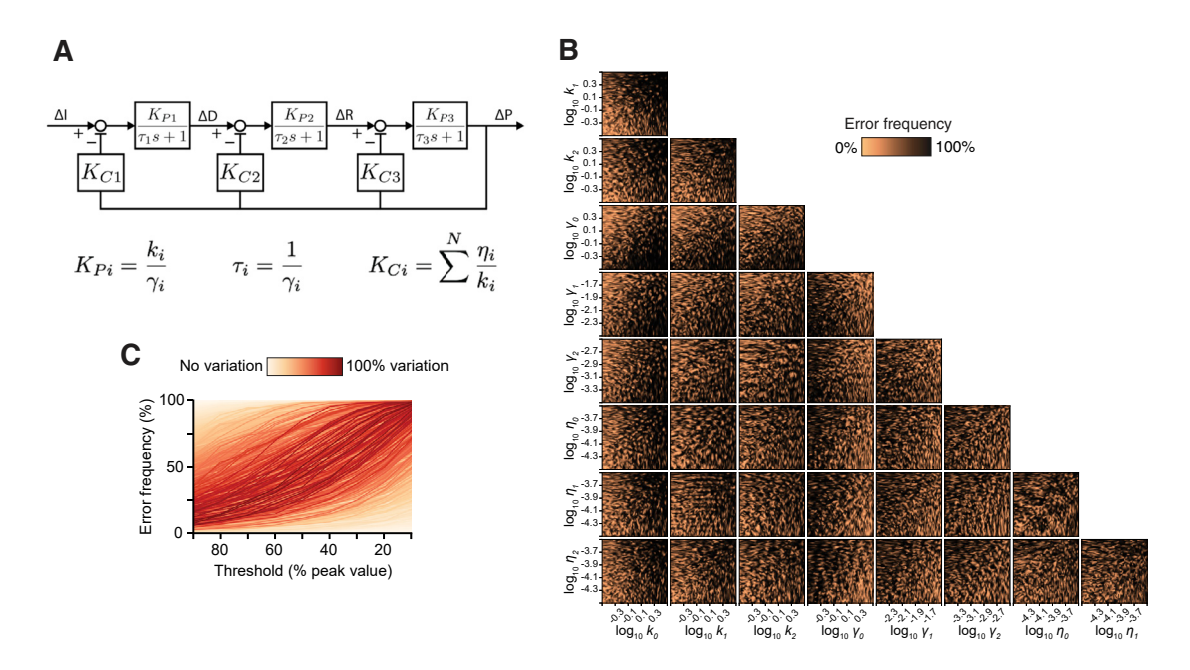


Figure S3. Model Demonstrating that Error Frequencies Are Broadly Increased When an Auxiliary Repressor Is Lost, Related to Figure 4

(A) Control theoretic depiction of the mathematical model. Arrows represent the flow of biochemical information, boxes contain transfer functions relating upstream and downstream signals, open circles indicate summation points. Transfer functions are expressed in the Laplace frequency domain.

(B) Each of the nine model parameters was varied by one order of magnitude centered around the default value as defined in the STAR Methods. Simulations with full and partial post-translational repression were performed, and error frequencies with partial repression were calculated using a threshold of 30% peak. Shown is a grid of all 36 pairwise combinations of parameter variations. Error frequencies are projected as color heatmaps on the 36 squares. Error frequencies are high (dark brown) for most combinations of parameter values.

(C) The error frequencies for all parameter sets from (B) were calculated over a range of threshold values. The minimum and maximum of the threshold range was 10% and 90% of mean peak value. Shown are error frequencies incurred by partial repression. Each line represents one of the parameter sets from (B). The color of each line reflects the extent that error frequency varies as a function of the threshold value. The darkest lines are those parameter sets whose error frequency varies the most with the threshold. Error frequencies are much greater than zero no matter where the threshold is set.

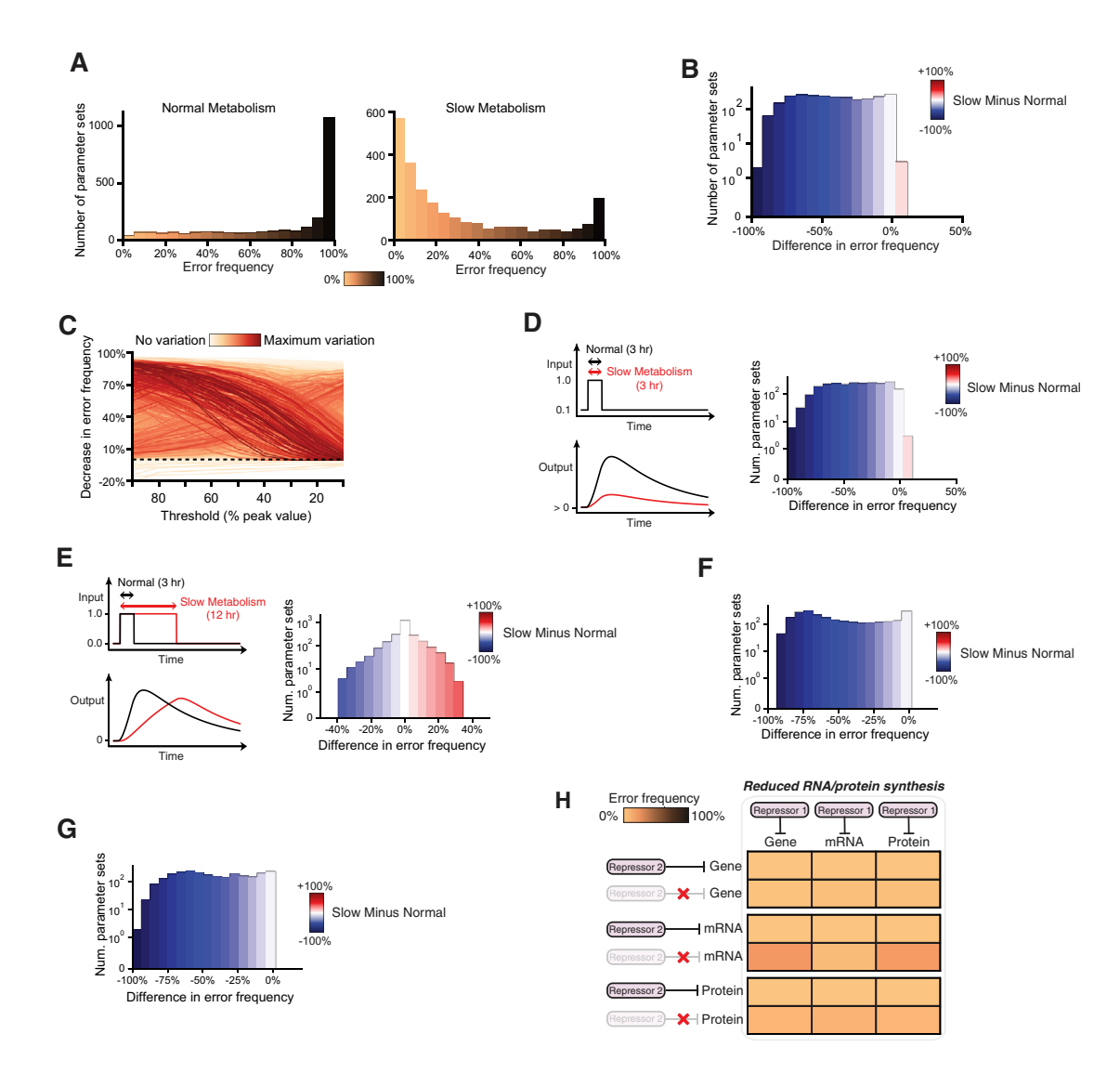


Figure S4. Reduced Energy Metabolism Diminishes the Importance of Repressors over a Wide Range of Model Conditions, Related to Figure 4

(A–G) Each of the nine model parameters was varied by one order of magnitude centered around the default value as defined in the STAR Methods. Simulations with full and partial repression were performed for each parameter set.

- (A) Distribution of error frequency for all parameter sets under conditions of normal or slow energy metabolism.
- (B) Distribution of the difference in error frequency between slow versus normal metabolism for all parameter sets.
- (C) The error frequency differences for all parameter sets from (B) were calculated over a range of threshold values. The minimum and maximum of the threshold range was 10% and 90% of mean peak value. Shown are error frequency differences incurred by slow metabolism. Each line represents one of the parameter sets from (B). The color of each line reflects the extent that error frequency difference varies as a function of the threshold value. The darkest lines are those parameter sets whose difference varies the most with the threshold. The vast majority of parameter sets exhibit some reduction in error frequency across all thresholds. (D–G) Systematic modification of model conditions showing the difference in error frequency between slow versus normal metabolism for all parameter sets. (D) Model where a nonzero basal stimulus is applied. (E) Model where input duration is increased four-fold by slow metabolism. (F) Model where an upper bound is placed on the number of sites firing transcription. (G) Model where cooperative transcription kinetics are considered. (H) Partial repression imparts few errors when RNA and protein synthesis rate parameter values are reduced by 50%.

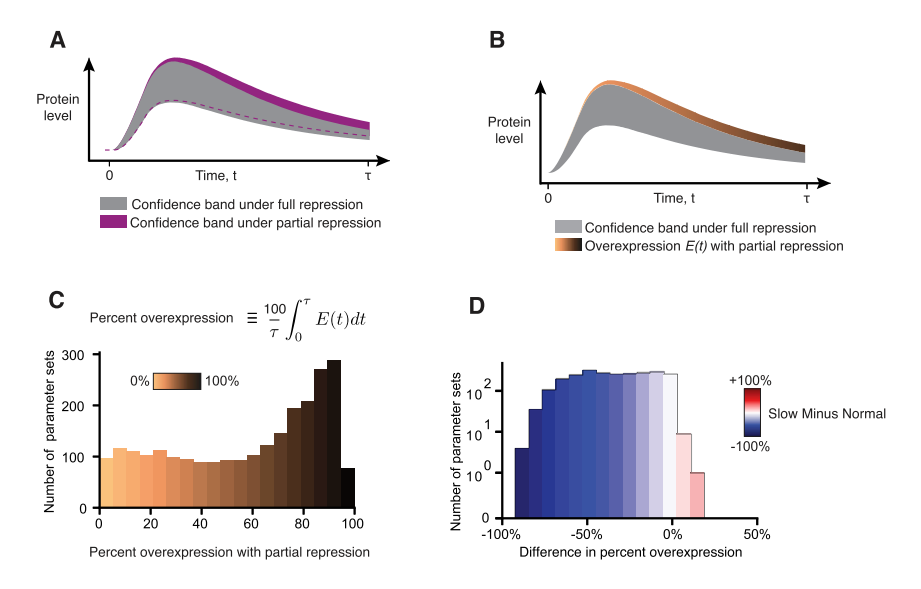


Figure S5. Reductions in Energy Metabolism Limit the Extent to which Protein Expression Dynamics Are Affected by Loss of a Repressor, Related to Figure 5

(A) Confidence bands span the 1st to 99th quantiles of protein trajectories simulated under full repression (gray) and partial repression (purple). The dashed purple line denotes the lower bound of the purple confidence band. The symbol τ denotes the commitment time as defined previously. (B) Partial repression causes overexpression E(t), which is the fraction of simulations that exceed the confidence band observed under full repression (gray) at a given time point t. Orange-brown color scale reflects the value of E(t) for each time point. (C) Percent overexpression caused by loss of a repressor for model simulations performed with 2500 independent parameter sets. Percent overexpression is the fraction of simulations that exceed the confidence band, averaged over the entire time course. A maximum of 100% overexpression would occur when all simulations exceed the confidence band at all time points. Overexpression is large for most parameter sets. (D) Distribution of the difference in percent overexpression between slow versus normal metabolism for all parameter sets. For the majority of parameter sets, overexpression is greatly reduced when energy metabolism is slow.

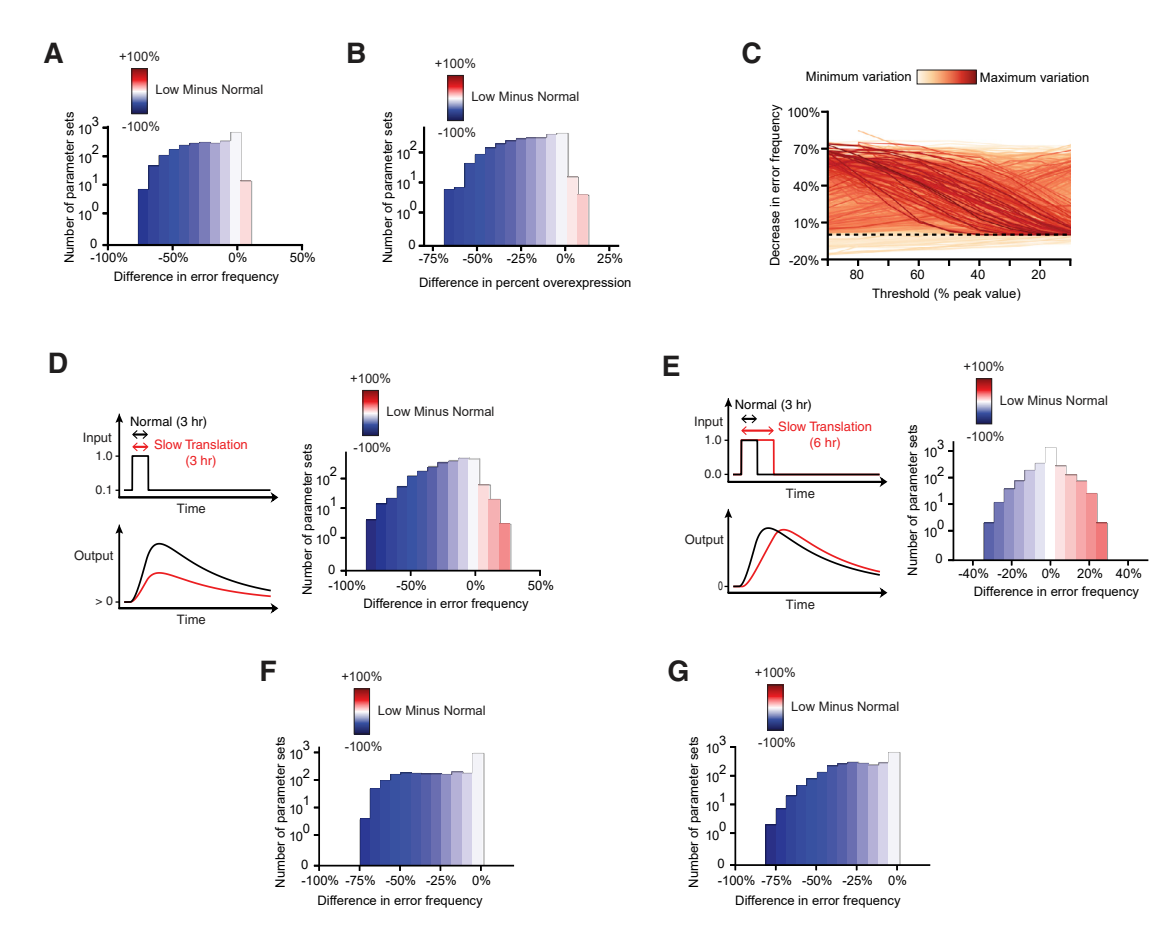


Figure S6. A Reduced Protein Synthesis Rate Diminishes the Effects of Repressor Loss over a Wide Range of Model Conditions, Related to Figure 7

Each of the nine model parameters was varied by one order of magnitude centered around the default value as defined in the STAR Methods. Simulations with full and partial repression were performed for each parameter set. (A) Distribution of the difference in error frequency between normal versus low rates of protein synthesis for all parameter sets. (B) Distribution of the difference in percent overexpression between normal versus low rates of protein synthesis for all parameter sets. (C) The error frequency differences for all parameter sets from (A) were calculated over a range of threshold values. The minimum and maximum of the threshold range was 10% and 90% of mean peak value. Shown are error frequency differences incurred by low rates of protein synthesis. Each line represents one of the parameter sets from (A). The color of each line reflects the extent that error frequency difference varies as a function of the threshold value. The darkest lines are those parameter sets whose difference varies the most with the threshold. The vast majority of parameter sets exhibit some reduction in error frequency across all thresholds. (D-G) Systematic modification of model conditions showing the difference in error frequency between normal versus low rates of protein synthesis for all parameter sets. (D) Model where a nonzero basal stimulus is applied. (E) Model where input duration is increased two-fold by low rates of protein synthesis. (F) Model where an upper bound is placed on the number of sites firing transcription. (G) Model where cooperative transcription kinetics are considered.